Geochronology, geochemistry and tectono-magmatic evolution of the upper Carboniferous–lower Permian Kula pluton in the Istranca (Strandja) Massif, NW Turkey

SERDAR AKGÜNDÜZ[1,✉], NAMIK AYSAL[1], IRENA PEYTCHEVA[2],
SABAH YILMAZ ŞAHİN[1] and YILDIRIM GÜNGÖR[1]

[1]Istanbul University – Cerrahpaşa, Engineering Faculty, Department of Geological Engineering, 34320, Istanbul, Turkey;
✉serdar.akgunduz@istanbul.edu.tr
[2]Department of Geochemistry and Petrology, Geological Institute, Bulgarian Academy of Sciences, BG-1113 Sofia, Bulgaria

Abstract: Upper Carboniferous–lower Permian plutonic rocks (i.e. the Kula pluton) are exposed in Istranca (Strandja) Zone, NW Pontides on both sides of Turkish and Bulgarian border. The Kula pluton is composed of monzogranite, granodiorite, and quartzmonzodiorite facies with a medium to coarse-grained, mylonitic–blasto mylonitic texture. It was affected by low-grade greenschist facies metamorphism, and displays distinct foliation as a result of intense tectonism. This pluton was classified as metaluminous and peraluminous (ASI values 0.95–1.13), I-type, calc-alkaline to high-K calc-alkaline in character. Zircon U–Pb crystallization ages of the pluton are between 298.0.6±0.68 Ma (early Permian – Asselian) and 311.91±1.34 Ma (late Carboniferous – Moscovian). Based on new geochemical and geochronological data, the Kula pluton was generated from a subduction-related magmatic arc-setting during the late Carbonifierous to early Permian. This period corresponds to the closure of the Paleo-Tethys Ocean following northward subduction of the Paleo-Tethyan oceanic lithosphere and development of a magmatic arc along the Eurasian continental margin.

Keywords: Kula pluton, Istranca Zone, geochemistry, geochronology, Paleo-Tethys.

Introduction

The Istranca massif is located in the northwestern part of Turkey, called the western Pontites, within the Alpine–Himalayan orogenic belt (Okay & Tüysüz 1999). The western continuation of the Istranca Massif was described as the Rhodope and the Serbo-Macedonian Massif (Fig. 1), and these massifs lie within the inner parts of Bulgaria and Greece (Chatalov 1988; Yanev 2000; Natal'in et al. 2005a, b; Natal'in 2006; Sunal et al. 2006; Fig. 1). These pre-Alpine metamorphic basement rocks are quite similar to each other in terms of degree of metamorphism and magmatic processes, and these features can be correlated with the Sakarya zone of western Turkey and the Pelogonian zone in northern Greece (Bonev et al. 2021 and references therein). The Rhodope and Istranca massifs are bounded by the Thrace Basin in the south (Okay et al. 2001). While these massifs are separated from the Sredna Gora zone by the Balkan reverse fault in the north, they are separated from the Istanbul Zone by the Western Black Sea fault in the east (Okay et al. 2001).

The Istranca Massif includes different sedimentary and magmatic rocks in terms of tectonic setting, degree of metamorphism, age, protolith and structural features (Aydın 1982; Chatalov 1988, 1991; Çağlayan & Yurtsever 1998; Okay et al. 2001; Sunal et al. 2011; Natal'in et al. 2012, 2016; Bedi et al. 2013; Yılmaz Şahin et al. 2014; Aysal et al. 2018a; Bonev et al. 2021 and references therein). The metamorphic units

forming the Istranca Massif are represented by sedimentary and igneous rocks that underwent poly-phase amphibolite and greenschist facies metamorphism, and were affected by intense deformation (Okay et al. 2001; Sunal et al. 2011; Natal'in et al. 2012, 2016). The rocks contain traces of different orogenic events (i.e. Cadomian, Variscan, and Alpine orogenic events: Burchfiel 1980; Liati 1986; Burg et al. 1990, 1996; Dinter & Royden 1993; Ricou et al. 1998; Liati & Gebauer 1999; Okay et al. 2001; Peytcheva et al. 2009, 2018; Natal'in et al. 2012, 2016; Yılmaz Şahin et al. 2012, 2014; Bedi et al. 2013; Machev et al. 2015; Aysal et al. 2018a; Bonev et al. 2019a, 2021; Yılmaz et al. 2021).

According to previous studies, first magmatic activity is represented by the Cadomian arc-related magmatism (Chen et al. 2002; Ustaömer et al. 2005; Okay et al. 2008; Yılmaz Şahin et al. 2009, 2014, Natal'in et al. 2016; Yılmaz et al. 2021). While the Precambrian–Cambrian magmatism in the Istranca massif ranges between 548.7±2.3 Ma and 506.1±4.5 Ma, it ranges between 560–590 Ma in the Istanbul zone (Chen et al. 2002; Ustaömer et al. 2005; Natal'in et al. 2016; Yılmaz et al. 2021). The second major magmatic activity is arc-related magmatism, formed by the northward subduction of Paleo-Tethys, represented by upper Carboniferous–lower Permian (320 to 271 Ma; Okay et al. 2001; Sunal et al. 2006; Natal'in et al. 2016; and this study) intrusive rocks, followed by backarc related middle Permian–Early Triassic magmatism (257–213 Ma) (Natal'in et al. 2006; Aysal et al. 2018a; Bonev
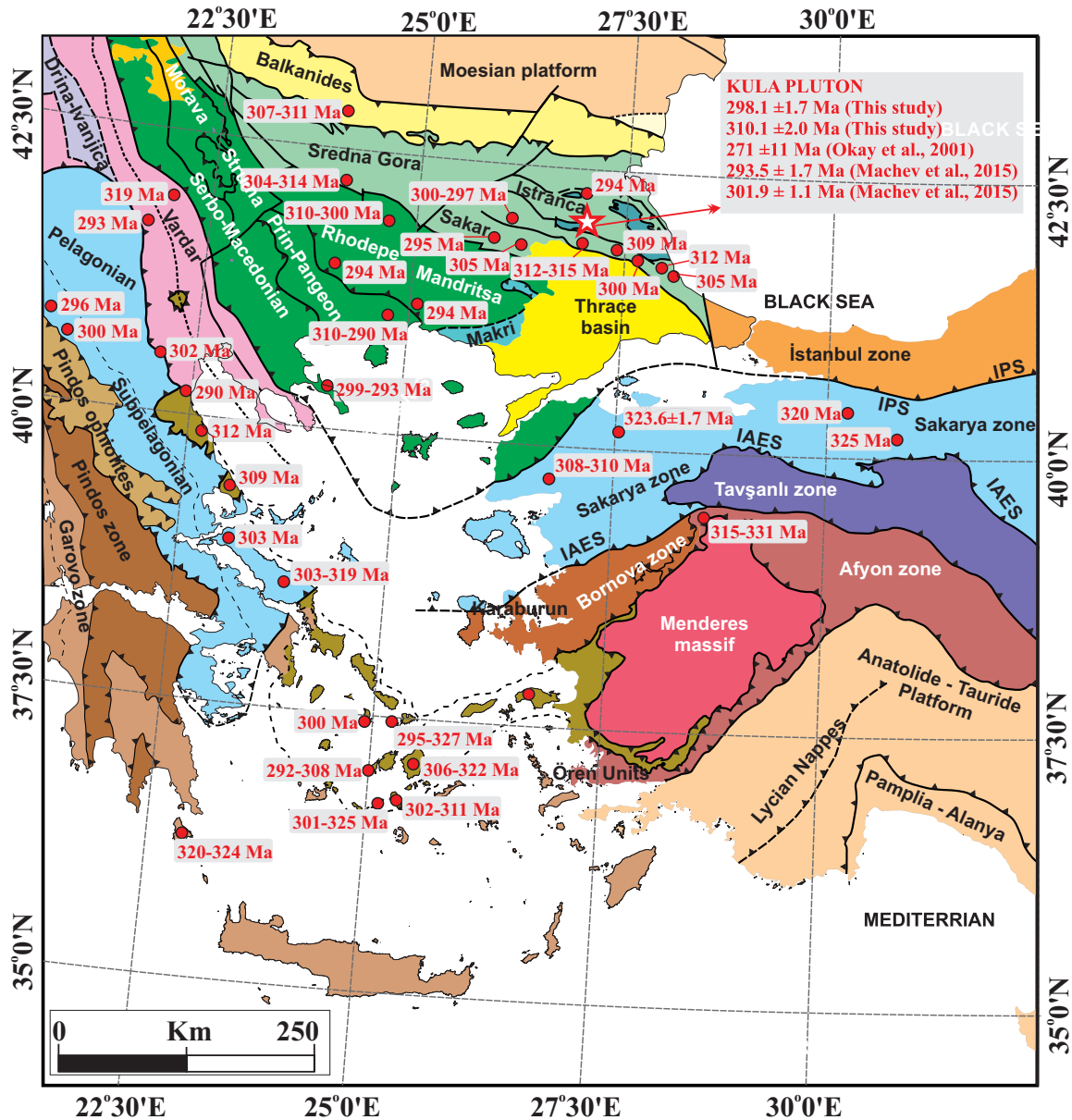
Fig. 1. Major tectono-stratigraphic units and suture belts of the Eastern Mediterranean region (modified from Okay & Tüysüz 1999; Bedi et al. 2013; Candan et al. 2016; Okay & Topuz 2017 and references therein). Age data references: Anders et al. (2007), Bonev et al. (2019a), Okay et al. (1996, 2001), Peytcheva et al. (2004; 2018), Sunal et al. (2006), Ustaömer et al. (2012), Xypolias et al. (2006), Zlatkin et al. (2014), Zulauf et al. (2014), Şengün et al. (2020), and this study. Abbreviations: IPS=Intra-Pontide suture, IAES=Izmir–Ankara–Erzincan suture, ITS=Inner-Tauride suture.

et al. 2021 and references therein). Late Carboniferous–early Permian magmatism was described in the Afyon Zone (331 to 315 Ma, Candan et al. 2016), and western–central parts of Sakarya Zone (336.3±2.9 Ma to 320 Ma, Okay et al. 1996; Ustaömer et al. 2016; Karslı et al. 2020; Şengün et al. 2020) (Table 1). The western continuation of late Carboniferous–early Permian magmatism was described in Bulgaria with a continuation in the Central Europe–Carpathian realm of Serbia and Romania. In Bulgaria granitoids outcrop in different regions, e.g., in Western Stara Planina (314±4.8 to 304.6 ±4 Ma, Dimitrov 1946; Carrigan et al. 2005 and Kamenov et

al. 2002), Sredna Gora (312±5.4 to 289.5±7.8 Ma, Zagorchev et al. 1973; Carrigan et al. 2006), Rhodope Massif (328 to 256±2.7 Ma, Peytcheva et al. 2004; Fakiya granite 301.9±1.1 to 293.5±1.7 Ma, Machev et al. 2015), Petrohan-Mezdreya (311.14±0.48 to 307.54±0.54 Ma, Peytcheva et al. 2018), and the Sakar unit (305 to 295 Ma, Bonev et al. 2019a; 297–295 Ma, Bonev et al. 2021). In addition, upper Carboniferous and early Permian sedimentary, volcanic, and subvolcanic magmatic rocks in Bulgaria were defined in the orogenic Balkanide Belt (Cortesogno et al. 2004; Vozárová et al. 2009). These late Carboniferous–Permian sedimentary

Table 1: Geochronological data from upper Carboniferous–lower Permian plutons in Turkey and Bulgaria.

Region	Method	Age (Ma)	References
Southern part of the Kula pluton (Turkey)	U–Pb	298.1±1.7, 310.1±2.0	**This study**
Southern part of the Kula pluton (Turkey)	Pb–Pb	271±11	Okay et al. 2001
Northern part of the Kula pluton (Bulgaria)	U–Pb	293.5±1.7, 301.9±1.1	Machev et al. 2015
Üsküp pluton in the Istranca Massif (Turkey)	Pb–Pb	309±24	Okay et al. 2001
Üsküp pluton in the Istranca Massif (Turkey)	U–Pb	299.1±2.7, 300.6±2.8	Natal'in et al. 2016
Vize Unit in the Istranca Massif (Turkey – Kaletepe Region)	U–Pb	311.3±3.1	Natal'in et al. 2016
Vize Unit in the Istranca Massif (Turkey – Kasatura Region)	U–Pb	312.5±2.4	Natal'in et al. 2016
Yavuzdere Unit in the Istranca Massif (Turkey – Yavuzdere Region)	U–Pb	303.6±2.5	Natal'in et al. 2016
Orthogneisses in the Istranca Massif (Turkey)	Pb–Pb	310 to 320	Sunal et al. 2006
Metagranites in the Sakarya Zone (Turkey)	U–Pb	325 to 320	Ustaömer et al. 2016
Metagranites in the Sakarya Zone (Turkey)	U–Pb	310 to 308	Okay et al. 1996
Felsic vein in the Central Sakarya Zone (Turkey)	U–Pb	319 ± 5	Topuz et al. 2020
Metagranite and amphibolite in the Central Sakarya Zone (Turkey)	U–Pb	378.8±10.2 to 418.75±6.5	Topuz et al. 2020
Metagranites in the Western Sakarya Zone (Turkey)	U–Pb	389.1±2.6 to 401.5±4.8	Aysal et al. 2012a,b
Metagranites in the Western Sakarya Zone (Turkey)	U–Pb	336.3±2.9	Şengün et al. 2020
Metagranites in the Central Sakarya Zone (Turkey)	U–Pb	403.9±3.5 to 405.9±2.5	Karslı et al. 2020
Metagranites in the Central Sakarya Zone (Turkey)	U–Pb	319.5±1.1 to 327.2±1.9	Ustaömer et al. 2012
Western Stara Planina (Bulgaria)		304.6 ±4	Dimitrov 1946
Western Stara Planina (Bulgaria)		314 ±4.8	Carrigan et al. 2005; Kamenov et al. 2002
Sredna Gora granites (Bulgaria)		289.5 ±7.8	Zagorchev et al. 1973
Sredna Gora granites (Bulgaria)	U–Pb	312 ±5.4	Carrigan et al. 2006
Rhodope Massif granites (Bulgaria)	U–Pb	328	Peytcheva et al. 2004
Petrohan–Mezdreya pluton (Bulgaria)	U–Pb	311.14±0.48, 307.54±0.54	Peytcheva et al. 2018
Sakar unit (Bulgaria)	U–Pb	305 to 295	Bonev et al. 2019a
Sakar unit (Bulgaria)	U–Pb	294.6±2.2	Bonev et al. 2021
Sakar unit (Bulgaria)	U–Pb	296.7±1.7	Bonev et al. 2021

sequences and volcanism in the Central Europe were compared with the Caucasus (Yanev & Adamia 2009).

The Kula pluton (southern part of the Kula pluton) is one of the upper Carboniferous–lower Permian plutons in the Istranca Zone (Fig. 2), and it is called the Fakiya Granite (northern part of the Kula pluton) on the Bulgarian site over the border (Machev et al. 2015). In previous studies, different ages were reported for the Kula pluton. The obtained ages are 271±2 Ma (Okay et al. 2001) and 301.9±1.1 to 293.5±1.7 Ma (Machev et al. 2015). Also, ages between 305 and 295 million years were obtained by Bonev et al. (2019a) from igneous rocks of the Sakar Unit. According to Dias & Ribeiro (1995), Okay et al. (2001), Weil et al. (2001), Abalos et al. (2002) and Martínez Catalán et al. (2009), the Kula pluton, Fakiya granite and granitoids of the Sakar Unit were evaluated as products of the Variscan orogeny, which developed as a result of the convergence and subsequent collision of two major paleocontinents, Laurasia and Gondwana, during the Late Paleozoic. However, Candan et al. (2016), and Bonev et al. (2019a) suggested that upper Carboniferous–lower Permian magmatic rocks in Turkey and Bulgaria were produced in a continental arc margins associated with northward subduction of Paleo-Tethyan oceanic lithosphere, rather than post-collisional or post-orogenic magmatism. Although Carboniferous magmatism is widely described in the Istranca Massif and the Central Sakarya Zone (Ustaömer et al. 2012; Natal'in et al. 2016; Topuz et al. 2020; Karslı et al. 2020), no Carboniferous magmatism is observed in the Istanbul zone, but significant Carboniferous zircon populations reported by Okay et al. (2011) in the upper parts

of the Istanbul Paleozoic Sequence (i.e. Trakya formation). Although Devonian magmatic activity was widely defined in the basement rocks of the Central Sakarya zone in a belt starting from the east of Kazdağ Massif and continuing to the north and east of Uludağ Massif (Okay et al. 2006; Aysal et al. 2012a,b; Sunal 2012; Karslı et al. 2020; Topuz et al. 2020) in Western Anatolia, Devonian magmatism was not described in the Istranca Massif. The third and final stage is formed by arc-related magmatism in the northward subduction of Neo-Tethys during the Late Cretaceous (Delaloye & Bingöl 2000; Karacık & Tüysüz 2010; Aysal et al. 2018b and references therein).

In this study, we present new zircon U–Pb geochronological and geochemical data from Kula pluton to interpret its origin and magmatic evolution. Furthermore, it is correlated with similar magmatic rocks in the Rhodope Massif, SE Bulgaria, and western Sakarya zone in Turkey. Consequently, the main purpose of the manuscript is to reveal the geodynamic setting and tectono–magmatic evolution of late Carboniferous–early Permian magmatism in the Istranca Zone.

Geological background

Regional geology

The basement rocks of the Istranca Massif are represented by the Cadomian arc-related meta-igneous rocks (Yılmaz Şahin et al. 2014; Natal'in et al. 2016; Yılmaz et al. 2021), and
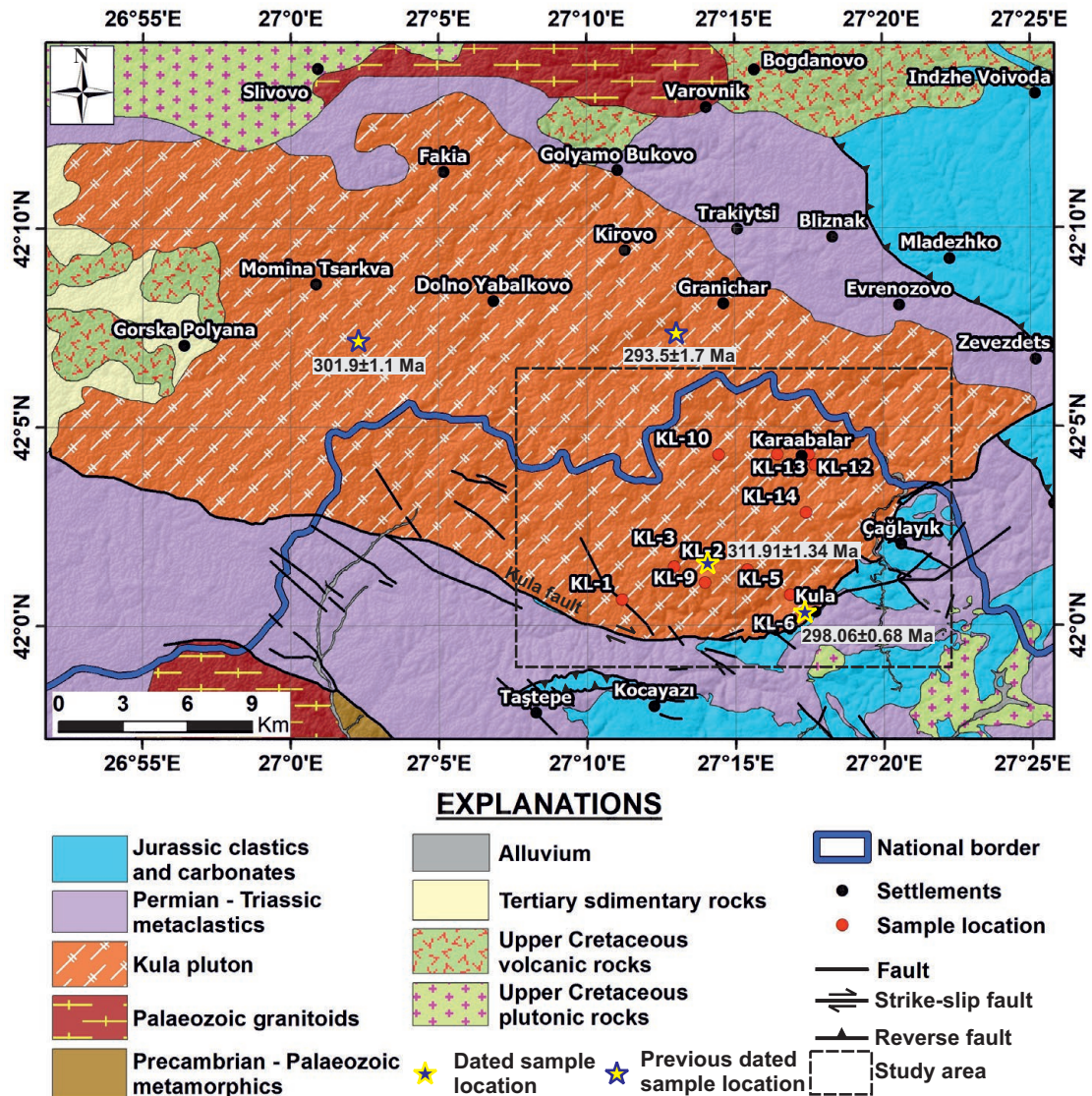
Fig. 2. Simplified geological map of study area (modified from Çağlayan & Yurtsever 1998; Machev et al. 2015; Akgündüz 2017; Geographic coordinate system WGS-84 datum).

meta-sedimentary rocks (i.e. Tekedere group; Bedi et al. 2013). These meta-igneous rocks are represented by the Çatalca (534.5±4.7 Ma to 546.0±3.9 Ma, Yılmaz Şahin et al. 2014), İhsaniye (535.5±3.6 Ma, Yılmaz Şahin et al. 2014), Kazandere (535.8±4.2 Ma to 542.6±3.5 Ma, Natal'in et al. 2016), Lala (546.4±4.7 Ma, Natal'in et al. 2016), Binkılıç (548.7±2.3 to 525.3±3.5 Ma, Yılmaz et al. 2021), Safaalan (543.3±2.8 to 534±2.6 Ma, Yılmaz et al. 2021), and Vize plutons (506.1±4.5 Ma, Natal'in et al. 2016). These rocks were covered by an Ordovician–Carboniferous metasedimentary complex (Natal'in et al. 2016). This metasedimentary complex includes the Tekedere Group, Koruköy and Evciler gneisses, and Kocabayır metaclastics.

Tekedere Group mainly consists of biotite schist, biotite–muscovite schist, amphibolite, quartz–chlorite–biotite–muscovite schist and gneisses (Çağlayan & Yurtsever 1998;

Natal'in et al. 2012; Bedi et al. 2013). The Kocabayır metaclastics consists of metaconglomerate, metasandstone, quartzite and rarely calc-schist. It outcrops in the western and central parts of the massif, and is cut by late Carboniferous plutons representing subduction-related characteristics (Natal'in et al. 2012, 2016). These plutons are described as the Üsküp metagranite (Okay et al. 2001; Natal'in et al. 2016), Kula pluton (this study) and orthogneiss (Sunal et al. 2006).

The Pb–Pb age from the Üsküp metagranite is 309±24 Ma (Okay et al. 2001), while U–Pb ages are 299.1±2.7 and 300.6±2.8 Ma (Natal'in et al. 2016). Reported Pb–Pb ages from the orthogneisses are from 310 to 320 Ma (Sunal et al. 2006). The U–Pb ages from the Kula pluton are 298.06±0.68 and 311.91±1.34 Ma in this study, respectively (Table 1). In addition, similar plutonic rocks formed in this period extend towards Bulgaria, Western Stara Planina, Sredna Gora,

Rhodope Massif, and Sakar unit. The metamorphic rocks of the Istranca Massif are cut by Permo–Triassic plutons (Okay et al. 2001; Aysal et al. 2018a), and covered by Triassic–Middle Jurassic metasedimentary sequences (Aydın 1974, 1982; Chatalov 1988, 1991; Çağlayan & Yurtsever 1998; Okay et al. 2001; Bedi et al. 2013). This metasedimentary sequence is a transgressive sequence that starts with metaconglomerates and metasandstones and transitions to carbonate rocks towards the top of the succession (Okay et al. 2001).

These cover units are cut by Late Cretaceous plutons (Demirköy pluton; Karacık & Tüysüz 2010), and are unconformably overlain by volcanic-sedimentary rocks around the İğneada region along the southern Black Sea coastline (Okay et al. 2001). Upper Cretaceous magmatism continued in the Istanbul zone (Delaloye & Bingöl 2000), and is represented by a pluton (i.e. Çavuşbaşı granodiorite; Yılmaz Şahin et al. 2012), mafic–intermediate dykes and volcanic counterparts (Aysal et al. 2018b and references therein). The Istranca Massif is separated from the Istanbul Paleozoic units by a tectonic contact west of Istanbul (near Çatalca), and it is covered by sedimentary rocks of the Thracian Basin in the south.

Field geology and petrography

The Kula pluton outcrops on both sides of the border between Turkey (southern part of the Kula pluton) and Bulgaria (northern part of the Kula pluton) in the north-western part of the Istranca massif (Figs. 1 and 2). This pluton has an intrusive contact with the metamorphic basement rocks of the Istranca Zone, and is unconformably overlain by Triassic–Upper Cretaceous sedimentary rocks in the southern (Turkey) and northern (Bulgaria) parts of the pluton (Fig. 2; Machev et al. 2015). Metamorphic basement rocks are represented by migmatites, two-mica gneisses, leucocratic gneisses, marbles and amphibolites (Bedi et al. 2013).

The southern part of the Kula pluton is separated from the Triassic metasedimentary sequence by a fault zone (the Kula fault) around Kula village toward the Turkish–Bulgarian border (Fig. 2). This fault zone starts from east of Çağlayık Village, passes through Kula village, and extends towards the north of Terzidere village (Fig. 2). It can be observed approximately 20 km long at the surface, consisting of dextral strike-slip faults and oblique normal faults that strikes NE–SW and E–W. Because of the intense tectonism and deformation, the Kula pluton exhibits diverse textural features such as mylonitic–cataclastic textures, oblique foliation, and mineral lineations in different areas (Fig. 3).

The well-developed foliation is depicted by the planar arrangement of large K-feldspar porphyroclasts and biotite flakes (Fig. 3a, b), which are conform with the magmatic planar-linear and foliated structures in the host rock. The Kula pluton is a light coloured and medium- to coarse-grained pluton. The primary igneous texture of the pluton is partly preserved in some places, and quartz, plagioclase, and K-feldspar porphyroclasts can be observed in hand specimens (Fig. 3c).

The main mineral composition of the pluton consists of quartz (20–25 %), plagioclase (45–50 %), K-feldspar (10–20 %) and mica (muscovite, and biotite). The accessory mineral phase is represented by zircon, titanite, apatite and opaque minerals, and the secondary mineral phase is made up of chlorite, epidote, calcite, sericite, and clay minerals (Fig. 3d, e). Plagioclase is the dominant mineral in the pluton, being represented by coarse-idiomorphic-grains with albite and Carlsbad twinning (Fig. 3d). The boundaries of prismatic plagioclase are surrounded by small quartz grains and fine-grained white mica (sericite, muscovite), and rarely chlorite and epidote (Fig. 3d) due to dynamic recrystallization, which occurred along the plagioclase porphyroclasts (Fig. 3d, e). Also, plagioclase crystals are locally replaced by sericite, epidote, and calcite minerals. Quartz exhibits elongated bands including fine grains with undulose extinction, and sub-grain formation along the fault zones (Fig. 3e). Primary quartz crystals were recrystallized in quartz ribbons (Fig. 3e). In addition, the main foliation of the pluton is defined by the preferred orientation of the muscovite and biotite minerals.

K-feldspar porphyroclasts are characterized by small prismatic crystals, and their boundaries are replaced by small quartz, and mica minerals related to dynamic recrystallization. They also show weak perthitic structure especially in highly deformed porphyroclasts. In addition, rarely observed microcline is represented by large idiomorphic shapes with perthitic textures, and plagioclase, biotite, muscovite and sericite inclusions. Mica minerals are represented by small subidiomorphic grains, and turn into chlorite because of the low-grade metamorphism and/or alteration affecting the pluton. On the basis of the equilibrium mineral assemblages, it can be concluded that the degree of metamorphism is low-grade greenschist facies. Similar metamorphic effects were reported from the other plutons (i.e. Üsküp, Kırklareli, Düzoba, and etc.) in the Istranca Massif, the Fakiya granite, and metagranites of Sakar Unit on the Bulgarian side of the border (Okay et al. 2001; Machev et al. 2015; Bonev et al. 2019a).

Analytical methods

Major and trace element geochemistry

Whole-rock geochemistry analyses were carried out on fourteen samples taken from the Kula pluton (Table 2). Major, trace and rare earth elements were conducted at the ACME Analytical Laboratories, Canada. Major oxides were analysed by using an inductively coupled plasma atomic emission spectrometry (ICP-AES), and trace – rare earth elements were analysed by using an inductively coupled plasma mass spectrometry (ICP-MS). The major oxides had a detection limit of 0.01 %, while trace – rare earth elements had detection limits of 0.01–1 ppm. Major and trace element abundances were determined on 0.2 g aliquots of samples following $LiBO_2$ fusion and HNO_3 acid digestion. Loss on ignition (LOI) is
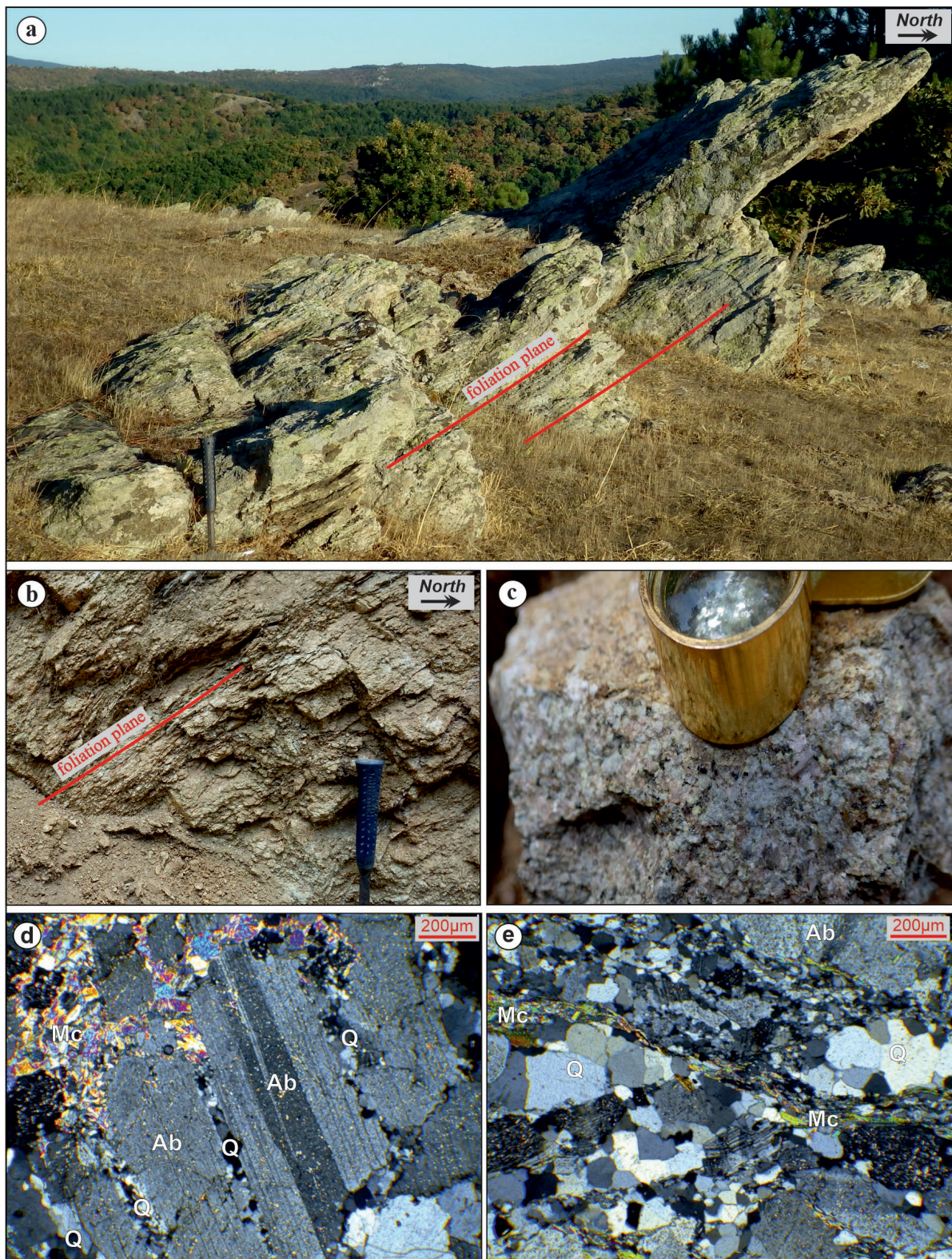
Fig. 3. a, b — Foliated and banded image of Kula pluton near tectonic lineaments (north of Kula village, location KL-14). **c** — Light-coloured, medium- to coarse-grained appearance of Kula pluton (location KL-3). **d** — Twinned prismatic plagioclase grains and small quartz grains along the long edge of plagioclase porphyroclasts (location KL-6). **e** — Quartz ribbons with aligned muscovite and biotite minerals along the main foliation plane (location KL 8). Abbreviations: Ab=albite, Q=quartz, Mc=mica.

the weight difference after ignition at 1000 °C. The results are given in Table 2.

U–Pb zircon dating

U–Pb geochronology analyses were carried out on two samples taken from the Kula pluton (Fig. 2). In order to determine the age of the pluton, two samples (Kl-2 and KL-6) were taken at different times and dated. In addition, the continuation of the pluton in Bulgaria was compared with the two age data (L1 and L2) produced by Machev et al. (2015). The zircon grains were separated by using traditional heavy liquid techniques after crushing, grinding, sieving and cleaning processes. The selected zircon grains were polished after mounting in epoxy resin, and its cathodoluminescence (CL) images were taken at the Belgrade University SEM laboratory using JEOL JSM-6610LV. CL images of the KL-2 sample were taken before analysis, and analysis was performed after the points were selected on the CL images. In the KL6 sample, however, Cl imaging was performed after analysis. The U–Pb isotope analyses were carried out at the Geological Institute of the Bulgarian Academy of Sciences in Sofia (Bulgaria) by using a Perkin-Elmer ELAN DRC-e ICP-MS with the NewWave UP-193FX 193 nm laser ablation unit attached. Generally, zircon grains between 150–250 μm in size were selected. GEMOC GJ-1 zircon standard was used as primary zircon reference material during the analyses. The results of the geochronological analyses calculated by using

Table 2: Results of whole-rock major (wt. %), trace and REE (ppm) for the Kula pluton.

	KL-1	KL-2	KL-3	KL-4	KL-5	KL-6	KL-7
Latitude	42.011222°	42.024925°	42.030156°	42.023525°	42.012967°	42.005553°	42.030869°
Longitude	27.186225°	27.215544°	27.221494°	27.256633°	27.280794°	27.288833°	27.221364°
SiO_2	59.32	66.45	75.09	74.58	75.14	69.20	62.89
Al_2O_3	17.15	16.83	12.78	12.92	12.91	16.25	16.47
Fe_2O_3	5.57	3.11	1.53	1.54	1.76	1.93	3.71
MgO	3.12	1.00	0.20	0.20	0.49	0.71	2.21
CaO	4.66	2.63	0.05	0.05	0.45	1.68	2.53
Na_2O	4.13	4.95	1.45	1.45	3.41	5.15	6.49
K_2O	2.60	2.17	8.12	8.28	4.62	3.12	1.59
TiO_2	1.02	0.55	0.17	0.17	0.25	0.23	0.82
P_2O_5	0.36	0.13	0.03	0.03	0.06	0.09	0.29
MnO	0.09	0.04	0.02	0.02	0.04	0.04	0.08
LOI	1.6	1.9	0.5	0.7	0.8	1.3	2.7
Sum	99.6	99.8	99.9	99.9	99.9	99.7	99.8
Ba	1336	995	414	427	277	1255	701
Sc	11	5	5	5	3	2	10
Ni	30.8	4.9	24.3	25.1	37.7	3.8	13.0
Co	13.8	8.0	1.6	1.3	2.6	3.5	8.1
Cs	0.6	1.7	1.5	1.9	0.8	0.4	0.1
Ga	22.7	19.6	14.0	14.7	17.0	15.2	16.5
Hf	5.5	3.8	5.2	5.7	4.8	3.1	5.9
Nb	14.1	7.1	11.3	11.3	11.0	4.5	6.4
Rb	76.0	67.1	351.9	367.3	223.8	68.8	35.2
Sr	968.8	848.7	50.7	56.1	81.7	591.9	369.2
Ta	1.6	0.6	1.1	1.2	1.5	0.5	0.5
Th	6.5	6.3	26.1	26.2	38.5	10.7	7.9
U	1.6	2.1	4.6	4.3	7.9	1.8	1.8
V	103	59	8	9	22	24	83
W	51.3	0.6	56.2	44.1	49.8	0.5	0.5
Zr	213.1	143.6	163.5	184.5	147.8	112.4	242.4
Y	29.3	13.4	17.2	18.6	33.6	10.3	14.4
La	36.6	28.2	27.1	26.1	36.0	31.4	46.1
Ce	91.4	70.8	93.6	93.5	71.0	57.1	81.1
Pr	12.94	7.81	6.70	6.62	8.23	6.17	9.84
Nd	54.3	30.2	23.7	23.4	28.7	21.8	36.9
Sm	11.29	5.38	4.48	4.59	5.66	3.49	6.14
Eu	2.57	1.38	0.32	0.32	0.49	0.72	1.52
Gd	8.63	3.84	3.84	3.83	5.34	2.35	4.66
Tb	1.22	0.53	0.56	0.57	0.87	0.32	0.56
Dy	6.24	2.63	3.48	3.43	5.27	1.72	2.88
Ho	1.05	0.48	0.68	0.80	1.13	0.37	0.51
Er	2.79	1.21	2.22	1.98	3.39	0.99	1.32
Tm	0.38	0.17	0.33	0.35	0.53	0.14	0.19
Yb	2.37	1.11	2.36	2.34	3.49	0.91	1.16
Lu	0.33	0.14	0.34	0.35	0.52	0.14	0.16

Table 2 (continued)

	KL-8	KL-9	KL-10	KL-11	KL-12	KL-13	KL- 14
Latitude	42.025928°	42.018233°	42.071814°	42.071839°	42.071928°	42.067403°	42.047372°
Longitude	27.234831°	27.232794°	27.240686°	27.273681°	27.291294°	27.294869°	27.289686°
SiO_2	60.26	65.43	71.18	74.22	75.02	71.08	65.93
Al_2O_3	17.16	16.05	15.15	14.55	12.89	14.49	17.09
Fe_2O_3	5.05	3.75	1.82	0.51	1.55	2.09	2.72
MgO	3.10	1.73	0.64	0.10	0.26	0.67	1.01
CaO	3.33	3.24	1.62	0.38	0.53	1.53	3.24
Na_2O	4.63	4.83	4.33	4.03	3.06	3.83	5.58
K_2O	2.90	2.12	3.60	5.49	5.47	3.68	1.94
TiO_2	0.81	0.59	0.28	0.05	0.22	0.24	0.49
P_2O_5	0.27	0.21	0.11	0.03	0.05	0.07	0.17
MnO	0.08	0.06	0.03	0.01	0.02	0.04	0.04
LOI	2.0	1.7	0.9	0.6	0.8	2.1	1.5
Sum	99.6	99.7	99.7	100	99.9	99.8	99.71
Ba	1453	999	1965	477	235	1257	1060
Sc	9	7	3	2	4	2	4
Ni	14.4	5.9	1.7	0.8	0.8	1.6	3.4
Co	11.9	7.8	2.5	0.4	1.0	2.2	4.2
Cs	0.4	1.0	0.4	1.2	1.2	0.9	0.2
Ga	19.9	18.4	14.6	15.7	14.6	14.8	20.0
Hf	5.2	5.2	2.3	1.8	5.0	3.9	4.5
Nb	6.0	6.6	3.6	7.8	9.2	6.7	4.7
Rb	66.2	58.1	63.6	114.5	192.5	72.6	38.9
Sr	642.7	826.3	667.9	161.4	67.4	293.2	1131.5
Ta	0.4	0.6	0.3	1.7	0.8	0.3	0.4
Th	7.5	9.4	8.3	8.4	34.7	15.9	6.2
U	2.0	3.2	2.6	2.5	6.9	1.6	1.4
V	95	68	28	8	12	21	45
W	0.5	0.5	0.5	0.5	0.5	0.5	0.5
Zr	207.6	182.0	79.2	32.9	151.5	136.9	171.4
Y	12.7	13.0	5.6	7.6	22.7	7.7	10.1
La	41.0	38.7	22.4	7.6	43.0	37.2	34.6
Ce	75.9	70.7	39.6	12.9	84.4	64.4	66.9
Pr	8.70	8.56	4.33	1.62	9.64	6.56	8.08
Nd	32.3	31.8	15.9	5.6	32.9	21.5	30.1
Sm	5.36	5.23	2.59	1.21	5.75	3.01	5.31
Eu	1.46	1.35	0.70	0.30	0.34	0.77	1.28
Gd	4.15	3.93	1.85	1.06	4.61	2.02	3.59
Tb	0.52	0.48	0.22	0.19	0.70	0.26	0.41
Dy	2.71	2.56	1.19	1.22	4.28	1.44	1.93
Ho	0.47	0.44	0.20	0.27	0.80	0.28	0.34
Er	1.34	1.19	0.54	0.88	2.54	0.80	1.01
Tm	0.18	0.17	0.07	0.14	0.35	0.12	0.13
Yb	1.06	1.12	0.53	1.08	2.48	0.79	0.87
Lu	0.16	0.17	0.07	0.15	0.38	0.12	0.12

ISOPLOTR (http://www.isoplotr.com/isoplotr/), and are given in Tables 3 and 4.

Results

Whole-rock geochemistry

The samples from the Kula pluton have variable contents of SiO_2 (59.32–75.14 wt. %), Al_2O_3 (12.89–17.15 wt. %), Na_2O (1.45–6.49 wt. %), K_2O (1.59–8.28 wt. %) and low contents of CaO (0.05–4.66 wt. %), TiO_2 (0.05–1.02 wt. %), P_2O_5 (0.03–0.36 wt. %) and MgO (0.10–3.12 wt. %). Some samples (KL-1, 2, 7, 8, 9, and 14) have low SiO_2 (59.32–66.45 wt. %)

ratios while others (KL-3, 4, 5, 6, 10, 11, 12, and 13) have higher SiO_2 (69.20–75.14 wt. %) ratios. The Kula pluton samples are intermediate to felsic magma character due to SiO_2 content (59.32–75.14 wt. %), and their magnesium number (Mg#=100×Molar MgO/(MgO+FeO)) between 20 and 55. Based on modal mineral compositions, the Kula pluton samples fall into the syenogranite, monzogranite, granodiorite, and quartzmonzodiorite fields (Fig. 4a) on the Quartz–Alkali Feldspar–Plagioclase (QAP) classification diagram of Streckeisen (1974). On the total alkali-silica versus SiO_2 (TAS) diagram (Middlemost 1994) for plutonic rocks, samples of the pluton plot in monzonite, quartzmonzonite, granodiorite, and granite fields (Fig. 4b). The aluminium saturation index (ASI) values of the Kula pluton vary between

0.95 and 1.13. On the A/NK (Al$_2$O$_3$/Na$_2$0±K$_2$O) versus A/CNK (Al$_2$O$_3$/CaO±Na$_2$O±K$_2$O) diagram (Shand 1947), the samples plot in the peraluminous, and metaluminous fields. They show mainly I-type and slightly S-type affinity (Fig. 4c). On the K$_2$O versus SiO$_2$ classification diagram of Peccerillo & Taylor (1976), samples from the Kula pluton fall into the calc-alkaline and high-K calc-alkaline fields (Fig. 4d).

Zircon U–Pb geochronology

An average of twenty–twenty-five zircon grains was separated from each sample for dating. Most of the selected zircon grains have euhedral prismatic shape, and are usually transparent, and light brown to honey-coloured. Their cathodoluminescence (CL) images (Fig. 5a,c) show that they are typically igneous zircon with fine oscillatory zoning that is

Table 3: Results of zircon LA-ICP-MS age determination for sample KL-2 from the Kula pluton.

KL-2	Isotope ratios									Age, Ma				Ratio
	^{207}Pb/^{235}U	2SE	^{206}Pb/^{238}U	2SE	RHO	^{208}Pb/^{232}Th	1SE	^{207}Pb/^{206}Pb	1 SE	^{207}Pb/^{235}U	2S	^{206}Pb/^{238}U	2S	Th/U
1r	0.3599	0.0252	0.04976	0.0014	0.40	0.0152	0.0007	0.0524	0.0019	312.14	9.41	313.05	4.3	0.474
2r	0.362	0.0326	0.04995	0.0016	0.36	0.0157	0.0008	0.0526	0.0024	313.7	12.2	314.21	4.91	0.416
4rc	0.3612	0.0284	0.04981	0.0014	0.36	0.0159	0.0007	0.0526	0.0021	313.1	10.6	313.36	4.3	0.426
5cr	0.3581	0.0226	0.04946	0.0014	0.45	0.0145	0.0007	0.0525	0.0017	310.8	8.45	311.21	4.3	0.651
5r-rec	0.3296	0.0790	0.04563	0.0036	0.33	0.0175	0.0018	0.0524	0.0064	289.3	30.2	287.6	11.1	0.153
7r	0.3807	0.0284	0.04996	0.0016	0.43	0.0148	0.0008	0.0553	0.0021	327.6	10.4	314.28	4.91	0.427
7cr	0.4401	0.0602	0.05911	0.0028	0.35	0.0207	0.0014	0.0540	0.0038	370.3	21.2	370.21	8.52	0.265
8rc	0.3817	0.0292	0.05114	0.0018	0.46	0.0150	0.0009	0.0541	0.0021	328.3	10.7	321.52	5.52	0.544
9r	0.3613	0.0402	0.04963	0.0024	0.43	0.0157	0.0012	0.0528	0.0030	313.2	15	312.25	7.37	0.156
10rc	0.3859	0.0286	0.04986	0.0020	0.54	0.0152	0.0010	0.0561	0.0021	331.4	10.5	313.66	6.14	0.652
10c	0.3568	0.0318	0.04924	0.0020	0.46	0.0147	0.0010	0.0526	0.0024	309.8	11.9	309.85	6.14	0.615
11r	0.3647	0.0388	0.05003	0.0022	0.41	0.0150	0.0011	0.0529	0.0029	315.7	14.4	314.71	6.75	0.238
11rc	0.3605	0.0248	0.04818	0.0022	0.66	0.0151	0.0011	0.0543	0.0019	312.59	9.25	303.34	6.77	0.722
13r	0.3671	0.0366	0.04864	0.0022	0.45	0.0150	0.0011	0.0547	0.0028	317.5	13.6	306.17	6.76	0.423
16r	0.3424	0.0232	0.04911	0.0016	0.48	0.0146	0.0008	0.0506	0.0017	298.99	8.77	309.06	4.92	0.209
17r	0.3682	0.0358	0.05071	0.0022	0.45	0.0165	0.0011	0.0527	0.0026	318.3	13.3	318.88	6.75	0.471
17rc	0.3708	0.0294	0.04921	0.0020	0.51	0.0152	0.0010	0.0547	0.0022	320.2	10.9	309.67	6.14	0.148
19tr	0.3449	0.0356	0.04864	0.0026	0.52	0.0164	0.0013	0.0514	0.0027	300.9	13.4	306.17	7.99	1.972
19c	0.3228	0.019	0.03875	0.00080	0.36	0.0060	0.0004	0.0604	0.0018	284.05	7.29	245.08	2.48	0.170
21r	0.355	0.0384	0.04818	0.0026	0.50	0.0153	0.0013	0.0534	0.0030	308.5	14.4	303.34	8	0.518
21rc	0.3527	0.0332	0.04831	0.0024	0.53	0.0144	0.0012	0.0530	0.0026	306.7	12.5	304.14	7.38	0.030

Table 4: Results of zircon LA-ICP-MS age determination for sample KL-6 from the Kula pluton.

| KL-6	Isotope ratios									Age (Ma)				Ratio
	^{207}Pb/^{235}U	2SE	^{206}Pb/^{238}U	2SE	RHO	^{208}Pb/^{232}Th	1SE	^{207}Pb/^{206}Pb	1 SE	^{207}Pb/^{235}U	2S	^{206}Pb/^{238}U	2S	Th/U
1r	0.388	0.038	0.0487	0.001	0.21	0.0177	0.0012	0.0549	0.0027	332.9	13.9	306.54	3.07	0.13
1c	0.694	0.046	0.0368	0.0016	0.66	0.0362	0.0026	0.1263	0.0024	535.2	13.8	232.97	4.97	0.27
3	0.388	0.036	0.0486	0.001	0.22	0.0203	0.0016	0.0545	0.0027	332.9	13.2	305.92	3.07	0.06
4	0.378	0.03	0.047	0.0008	0.21	0.0158	0.0009	0.0549	0.0021	325.6	11.1	296.08	2.46	0.11
7	0.368	0.032	0.0472	0.0008	0.19	0.0152	0.0007	0.0536	0.0024	318.2	11.9	297.31	2.46	0.21
10	0.3614	0.02	0.0461	0.0006	0.24	0.0157	0.0004	0.0551	0.0016	313.26	7.46	290.53	1.85	0.28
8c	0.779	0.16	0.0855	0.0046	0.26	0.0297	0.0019	0.0654	0.0060	584.9	45.7	528.9	13.7	0.28
11	0.401	0.026	0.0469	0.0008	0.26	0.0235	0.0014	0.0631	0.0021	342.37	9.42	295.46	2.46	0.24
13	0.519	0.028	0.0455	0.0008	0.33	0.0352	0.0010	0.0851	0.0024	424.48	9.36	286.83	2.47	0.16
15	0.36	0.036	0.049	0.0012	0.24	0.0173	0.0007	0.0553	0.0029	312.2	13.4	308.38	3.69	0.27
17	0.339	0.028	0.0483	0.001	0.25	0.0156	0.0008	0.0529	0.0022	296.4	10.6	304.08	3.07	0.15
21	0.335	0.046	0.047	0.0016	0.25	0.0157	0.0022	0.0538	0.0038	293.4	17.5	296.08	4.93	0.06
20	0.331	0.034	0.0474	0.001	0.21	0.0172	0.0017	0.0533	0.0028	290.3	13	298.54	3.08	0.06
19	0.351	0.04	0.0473	0.0012	0.22	0.0224	0.0021	0.0566	0.0033	305.5	15	297.92	3.69	0.07
24	0.339	0.03	0.0489	0.001	0.23	0.0157	0.0013	0.0523	0.0024	296.4	11.4	307.76	3.07	0.08
27	0.33	0.026	0.047	0.0008	0.22	0.0129	0.0007	0.0515	0.0021	289.57	9.92	296.08	2.46	0.14
28	0.351	0.032	0.047	0.001	0.23	0.0135	0.0009	0.0535	0.0024	305.5	12	296.08	3.08	0.15
32	0.345	0.026	0.0477	0.0008	0.22	0.0142	0.0004	0.0524	0.0020	300.95	9.81	300.39	2.46	0.30
33	0.378	0.032	0.0465	0.0008	0.20	0.0248	0.0023	0.0581	0.0026	325.6	11.8	293	2.46	0.08
35	0.612	0.06	0.0791	0.0036	0.46	0.0255	0.0011	0.0579	0.0024	484.8	18.9	490.7	10.8	0.23
5	0.462	0.038	0.0471	0.0012	0.31	0.0415	0.0024	0.0699	0.0031	385.6	13.2	296.69	3.69	0.06
9	0.323	0.05	0.0473	0.0016	0.22	0.0166	0.0016	0.0505	0.0040	284.2	19.2	297.92	4.92	0.14
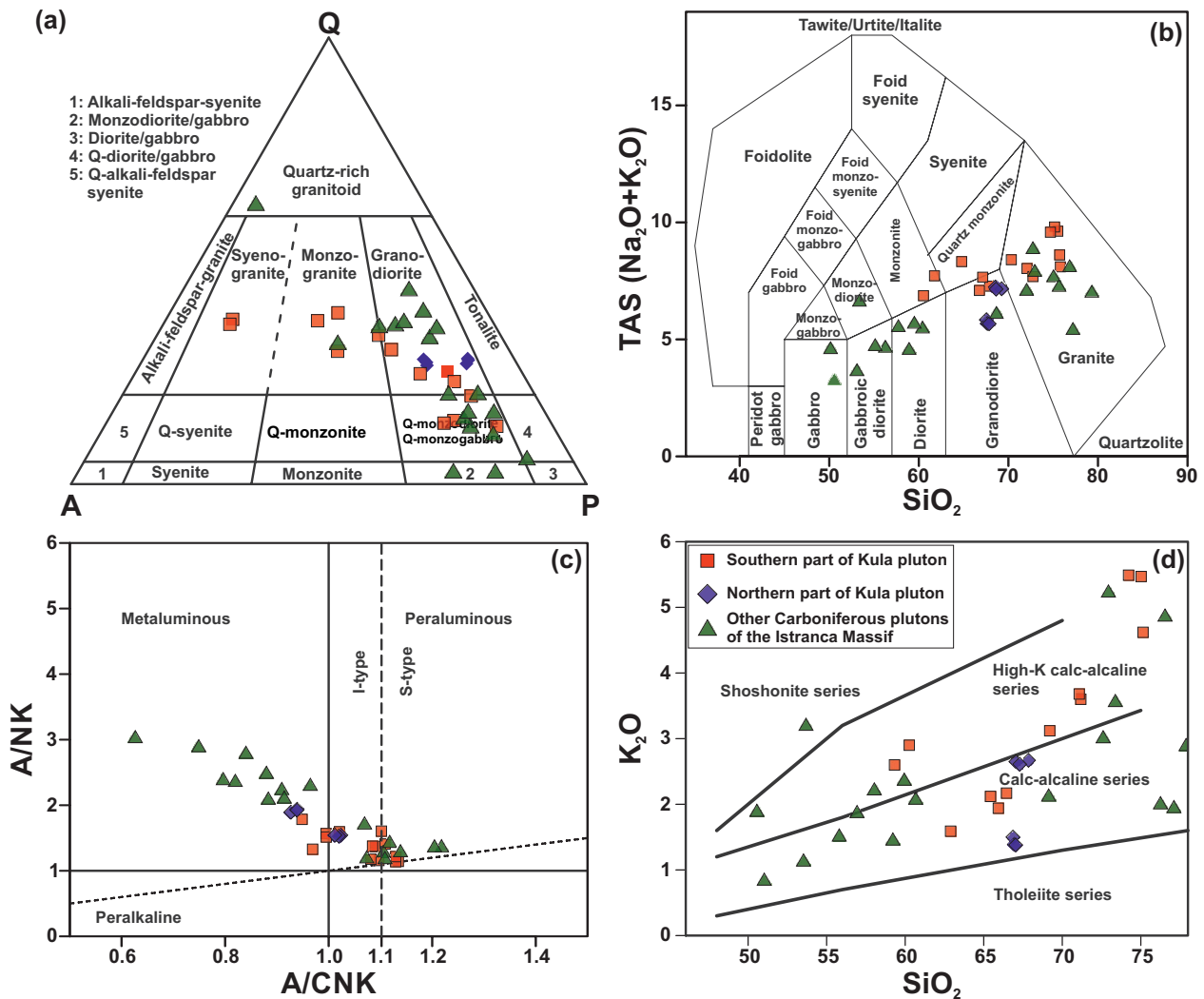
Fig. 4. a — QAP classification diagram (Streckeisen 1974) based on modal mineral composition. **b** — Total alkali versus silica (TAS) diagram (Middlemost 1994). **c** — A/NK–A/CNK diagram (Shand 1947; Maniar & Piccoli 1989). **d** — K_2O–SiO_2 diagram (Peccerillo & Taylor 1976) for the Kula pluton (geochemistry data for the other Carboniferous plutons of Istranca Massif and northern part of the Kula pluton were taken from Sunal et al. 2006 and Machev et al. 2015).

informative for high zirconium saturation (Hoskin & Schaltegger 2003). Although most zircons in our study are clearly igneous zircon, some zircon grains in KL-6 have bright CL spots and rims that are informative for solid-state or fluid-induced recrystallization around fractures, inclusions or in the outher parts of the crystals (Pidgeon 1992; Pidgeon et al. 1998; Corfu et al. 2003; Hoskin & Schaltegger 2003). Also, these samples have low Th/U values (Tables 3 and 4).

Sample KL-2

A total of twenty-one points were dated on fourteen selected zircon grains from the KL-2 sample. KL-2 sample yielded a population of zircons composed mainly of regular grains with few typical crystal faces (Fig. 5a). In CL images regular magmatic oscillatory growth zoning of KL-2 is dominant but

there is also evidence for resorption and over growth (Fig. 5a) or for changes in the chemistry of the magma (e.g., dark CL low-luminescent and trace-elemnt rich internal parts are followed by lighter parts). Twenty-one analyses of the KL-2 sample yielded $^{206}Pb/^{238}U$ ages ranging mainly from 303.34±6.77 Ma to 321.52±5.52 Ma (Fig. 5a) with few exceptions – one younger age related to Pb-loss from a U-rich part 245.08±2.48 Ma, and one inherited core dated at 370.21±8.52 Ma (Table 3 and Fig. 5a). Excluding the outliers and using all other analyses a concordia age of 311.91±1.34 Ma is defined (Fig. 5b).

Sample KL-6

A total of twenty-two points were dated on twenty-one selected zircon grains from the KL-6 sample. KL-6 sample has relatively sparse zircons that are generally short-prismatic and

relatively enriched in U (105–2370 ppm). Some grains do not show oscillatory zoning (Fig. 5c) or it is obliterated. Only one of the zircon grains has an inherited core age of 528.9±13.7 Ma (Table 4). This age is similar to the Cadomian magmatic events for the basement rocks of the Istranca Massif (Yılmaz Şahin et al. 2014; Okay & Nikishin 2015). Twenty-two analyses were made on zircons belonging to sample KL-6 from the cores and rims. The analyses yielded $^{206}Pb/^{238}U$ ages ranging generally between 286.83±2.47 Ma and 308.38± 3.69 Ma (Table 4, Fig. 5d) with two outliers, the latter either pointing to Pb-loss in the U-rich (dark in CL) parts (232.97± 4.97 Ma), or to inheritance (the Cadomian core with an age 528.9±13.7 Ma) (Table 4). Excluding the outliers, a concordia age of 298.06±0.68 Ma is calculated (Fig. 5d).

Discussion

Petrogenesis

The geochemical data of the Kula pluton has similar characteristics to some of the upper Carboniferous–lower Permian plutons in Turkey and the Istranca massif in the south-eastern part of Bulgaria (Sunal et al. 2006; Machev et al. 2015). We compared our new geochemical data with published data for these plutons. Upper Carboniferous–lower Permian plutonic rocks in western Turkey and SE Bulgaria were evaluated on Harker diagrams that show variations of major oxide values against SiO_2 values. The Kula pluton samples generally show compatible and complementary features on Harker diagrams
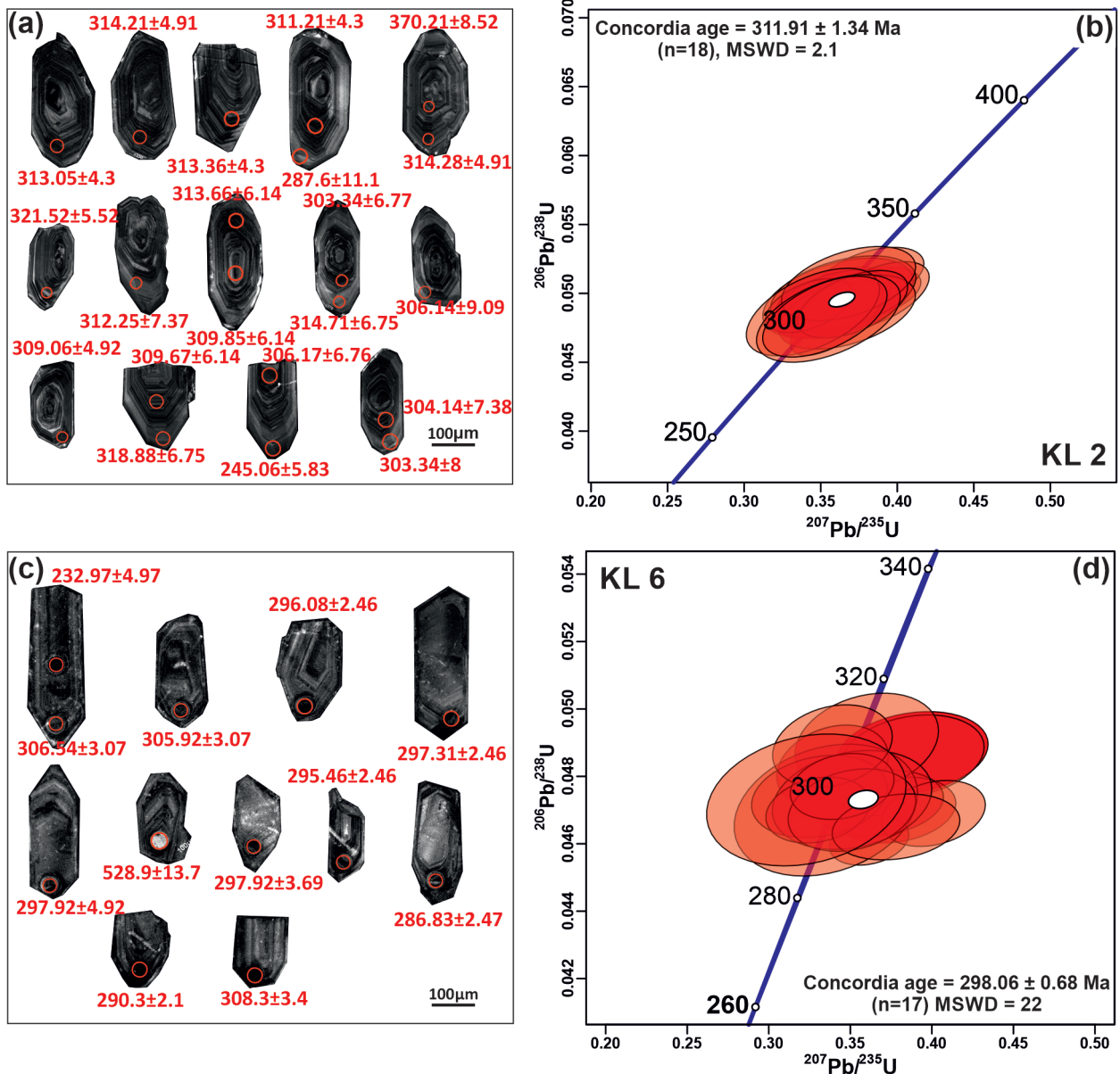
Fig. 5. a, c — CL images, and analysis points on zircon grains. b, d — Concordia diagrams for sample KL 2 and KL 6 from the Kula pluton.

compared with the other upper Carboniferous–lower Permian plutons in the Istranca Zone. Major oxides, and some trace elements versus SiO$_2$ Harker diagrams (Fig. 6) for the Kula pluton can be used to track some magma chamber processes (i.e. fractional crystallization (FC), and mixing). While Al$_2$O$_3$, Fe$_2$O$_3$, MgO, CaO, and TiO$_2$ contents of the pluton decrease with increasing SiO$_2$ contents, Na$_2$O and K$_2$O contents show disseminated patterns with increasing SiO$_2$ content. Similarly, the concentrations of Rb decrease with increasing SiO$_2$ contents, whereas sudden decreases in Ba and Sr over 70 wt. % SiO$_2$ indicates feldspar and accessory mineral crystallization. (Fig. 6). Despite the SiO$_2$ increase, the Sr content decrease (not shown in figure) can be explained by crystallization of

K-feldspar and plagioclase, while decreasing Ba content can be explained by crystallization of plagioclase, biotite and K-feldspar. The Rb content, which increases with increasing SiO$_2$, may indicate fractional crystallization and/or magma mixing events. Although the Zr and Nb elements generally present a scattered pattern, most of the samples fall between the lower and the upper continental crust values.

On the Nb versus Y, and Rb versus Y+Nb tectonic discrimination diagram (Pearce et al. 1984), samples for the Kula pluton (northern and southern parts), and other upper Carboniferous–lower Permian plutons of Istranca Massif mainly plot into the field of volcanic arc (VAG) and syn-collisional (syn-COLG) granites (Fig. 7a). Also, a very small
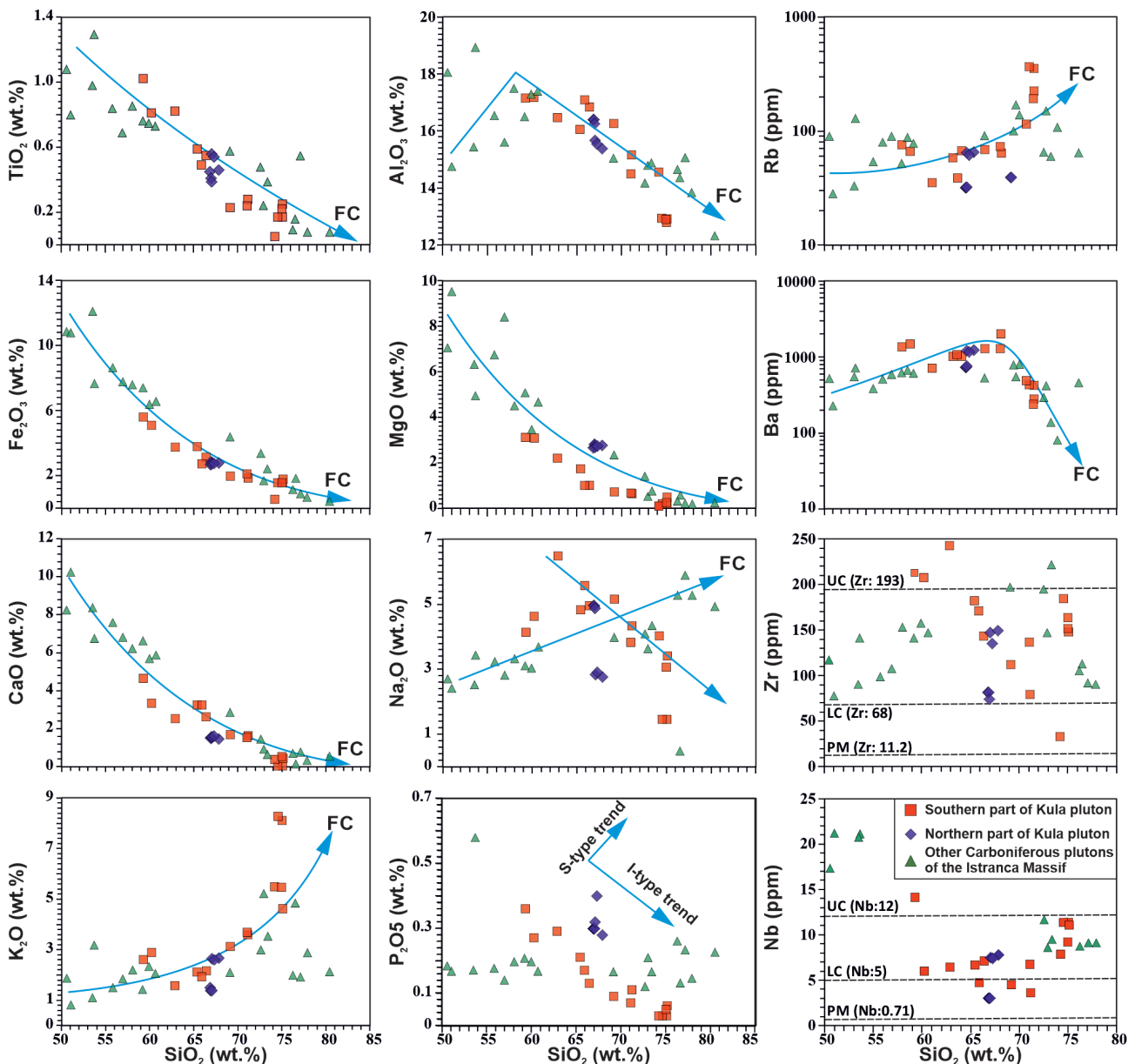
Fig. 6. Harker variation diagrams for major and some trace elements with SiO$_2$ for the Permo–Carboniferous plutonic rocks (I- and S-type trends taken from Chappell & White 1992; Lower Crust (LC) and Upper Crust (UC) values are from Rudnick & Gao 2003; Primitive Mantle (PM) values are from (Sun & McDonough 1989).
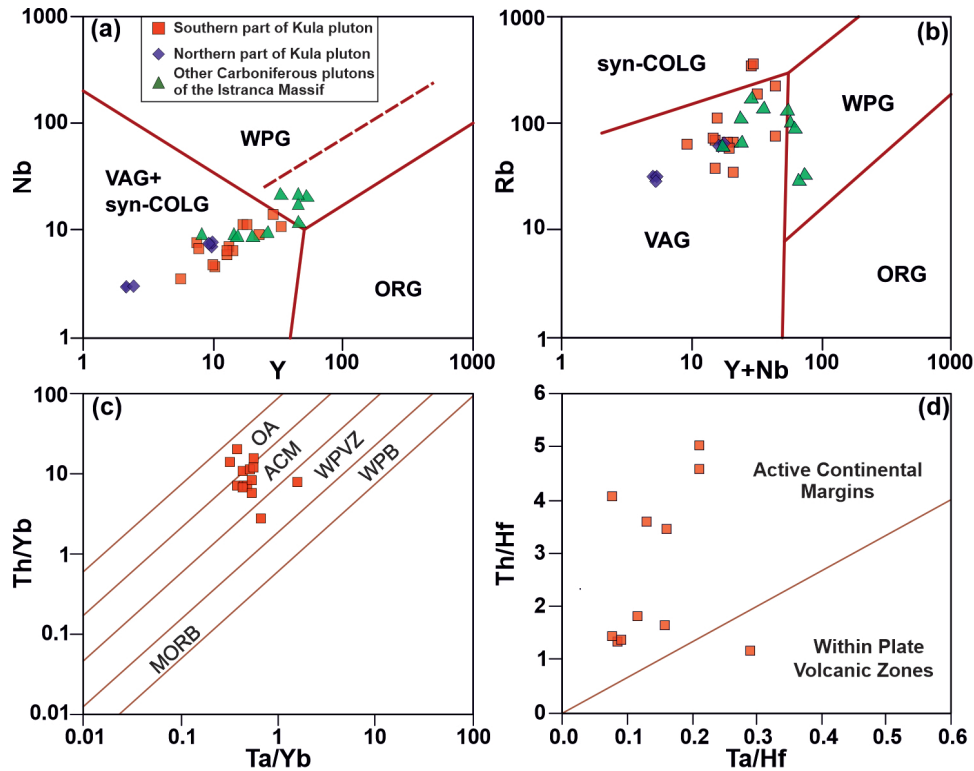
Fig. 7. Tectonic discrimination diagrams of the studied plutons: Nb versus Y (**a**) and Rb versus Y±Nb (**b**) diagrams of Pearce et al. (1984); Th/Yb versus Ta/Yb (**c**), and Th/Hf versus Ta/Hf (**d**) diagrams of Schandl & Gorton (2002). Abbreviations: MORB=mid-ocean ridge basalts; VAG=volcanic arc granites; ORG=ocean ridge granites; WPG=within plate granites; syn-COLG=syn-collisional granites; WPVZ=within plate volcanic zone; ACM=Active Continental margin; OA=Oceanic arc; WPB=within plate basalt.

number of samples of these plutons plot into the within-plate granite (WPG) on the Rb versus Y+Nb discrimination diagram (Fig. 7b). In addition, using the Th/Yb versus Ta/Yb, and Th/Hf versus Ta/Hf tectonic discrimination diagrams of Schandl & Gorton (2002), samples from the Kula pluton clearly fall in the field of the active continental margin (ACM) and oceainic arc (OA) except for two samples falling into the within plate volcanic zone (WPVZ) (Fig. 7c, d).

The Kula pluton samples were evaluated on multi-element and REE spider diagrams normalized to N-MORB, Lower Crust, Upper Crust, and Chondrite in order to investigate the properties of the source from which the magma was derived (Fig. 8). In the N-MORB normalized multi-element spider diagram (Fig. 8a), all samples of the Kula pluton show enrichment of large ion lithophile (LIL) elements (Sr, K, Rb, Ba and Th) and relatively depletion of high field strength (HFS) elements (Nb, Y, Ta, Ti). At the same time, prominent Ta, Nb, P and Ti negative anomalies can be observed in all samples. On this diagram, the Kula pluton displays a subduction-related signature of relatively enriched LIL elements with relatively depleted HFS elements (Ta and Nb) (Fig. 8a). High incompatible element abundances (e.g., K, Rb, and Ba) and strong depletions of Sr, Ta, Nb, P and Ti are also typical of subduction zone enrichment, assimilation and crustal contamination. In the Lower Crust – normalized diagram (Fig. 8b), all of the trace elements show similar trends with the N-MORB

normalized patterns. Although all trace elements in the Lower Crust normalized spider diagram show similar patterns to N-MORB, in the Upper Crust normalized spider diagram, almost all elements follow a horizontal trend in accordance with the Upper Crust values (Fig. 8c).

Chondrite-normalized rare-earth element diagram for the Kula pluton show enriched light rare earth elements (LREE) and flat HREE trend (Fig. 8d). Kula pluton samples show two different behaviours in terms of Eu anomaly (Eu/Eu* values are between 0.2 and 0.98). Some of the samples show strong negative Eu anomalies (KL-3, 4, 5 and 12), while others exhibit slightly negative Eu anomalies. These samples contain common feldspar minerals, such as plagioclase and orthoclase, and have been affected by sericitic alteration (Fig. 3d, e).

Eu anomalies are controlled by feldspar crystallization in igneous rocks and may be due to fractional crystallization of plagioclase and contamination from continental crust derived melts that has undergone considerable Eu consumption. It is seen that the samples, except for a few, follow a horizontal trend in the SiO_2 versus Eu/Eu* diagram (Fig. 9a). This may be a reflection of magma mixing and / or source melting rather than plagioclase fractionation. The fractional crystallization process is modelled on Ba versus Eu, Ba versus Sr, and Rb versus Sr and Ba binnary plots (Fig. 9b–d) by using the FC-Modeler excel spreadsheet (Keskin 2002). In the model, the Kd values for plagioclase, K-feldspar, biotite and

amphibole are those for felsic magma compositions. On the Ba versus Eu and Ba versus Sr diagrams, the increase in Ba contents with increasing Eu and Sr concentrations is possibly related to the fractionation of K-feldspar, while the decrease in Rb contents with increasing Sr concentrations is due to the fractionation of K-feldspar and plagioclase. However, on the Rb versus Sr diagram, the decrease in Rb contents with increasing Sr concentrations is possibly reflected to the fractionation of K-feldspar and plagioclase with biotite (Fig. 9d). At the same time, Permo–Carboniferous plutons in the Istranca Massif and northern part of the Kula pluton show compatible trends with the sothern part of the pluton. The Th/Nd versus Th diagram is a useful tool for monitoring magma mixing, partial melting and fractional crystallization processes. In this diagram, it is seen that majority of the samples are mostly aligned along the magma mixing and partly along the partial melting line rather than fractional crystallization line (Fig. 9e). Consequently, these geochemical trends from the Kula pluton must be produced by different degrees of magma mixing and/or partial melting. It defines curving arrays, which can be interpreted as mixing hyperbolas. Furthermore, the data on straight lines are discernible from mixing of sources (i.e. source contamination or metasomatism) (Schiano et al. 2010). Assimilation and fractional crystallization (AFC) process is modelled on Nb vs Nb/Zr diagram (Fig. 9f) by using the AFC-Modeler excel spreadsheet (Keskin 2013). The calculated vectors show that the pluton samples plot along a slightly linear trend from the BEM to assimilant, which can be interpreted as the assimilation is much more prominent regarding to the fractionation processes (r (Ma/Mc)=0.0–0.4). Trace element modelling shows that the Kula pluton is consistent with magma mixing, fractional crystallization and partial melting processes. Magma mixing of chemically contrasting compositions produces intermediate magmas in some arcs (e.g., Kuno 1950; Anderson 1976). Zaraisky et al. (2008) suggested that the Zr/Hf ratio in a granite intrusion related to single magma chamber regularly changes from granodiorite to biotite granite, leucogranite and Li–F granite (from 45–30 to 10–2) during the fractional crystallization processes. According to the Zaraisky et al. (2008) diagram (Fig. 9g), it is seen that the Kula pluton is located in the area of Barren granites, which gradually evolved from a mafic end member to leucogranites in accordance with the crystallization processes, and it can be said that these granites are poor granites in terms of Sn–W–Mo–Be mineralization.

Experimental petrology studies on different rock types have provided important clues in determining the primary source of the granitic magmas (Patiño Douce 1999; Altherr et al. 2000; Altherr & Siebel 2002; Castro et al. 2010; Laurent et al. 2014). Mg# values in Kula metagranitoid rock samples are between 20–55 and can be generated by crustal material with involvement of a mantle component. On the Mg# versus SiO_2 and molar Al_2O_3/(MgO+FeO$_T$) versus CaO/(MgO+FeO$_T$) diagrams (Fig. 10a,b) of Altherr & Siebel (2002), samples of the Kula pluton plot within the fields of melts derived from metabasalt, metaandesite, metapelite and metagreywacke
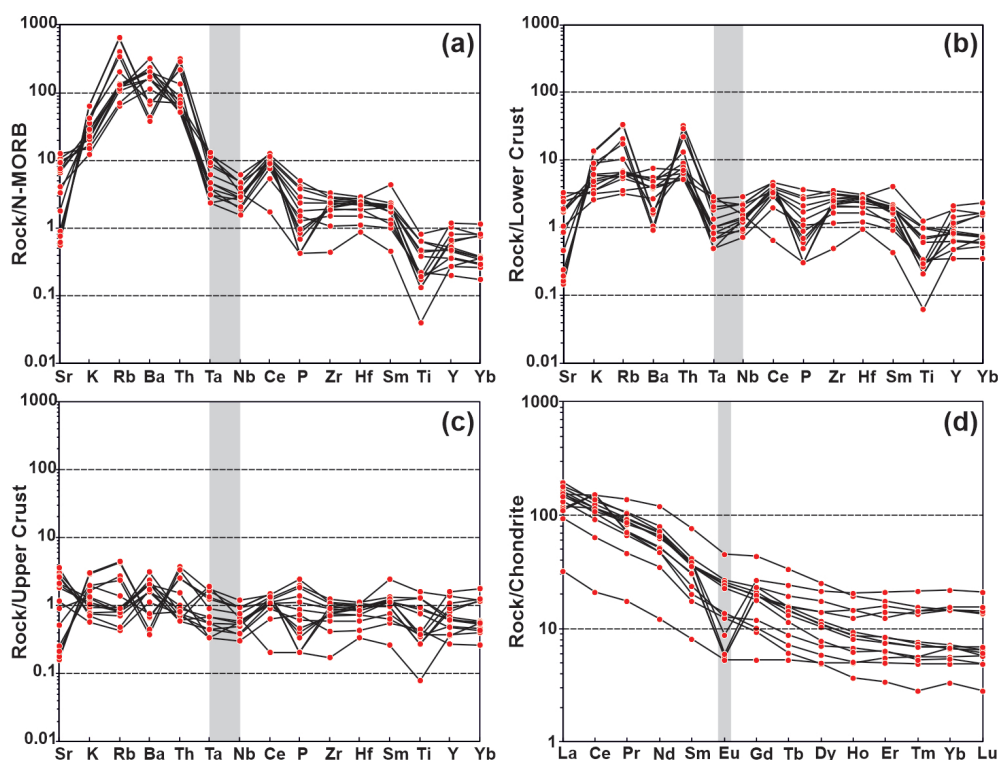

Fig. 8. N-MORB (**a**), Lower Crust (**b**), Upper Crust normalized multi-element (**c**), and Chondrite normalized REE (**d**) spider diagrams for the Kula pluton (normalization values are from Rudnick & Gao 2003; Sun & McDonough 1989).
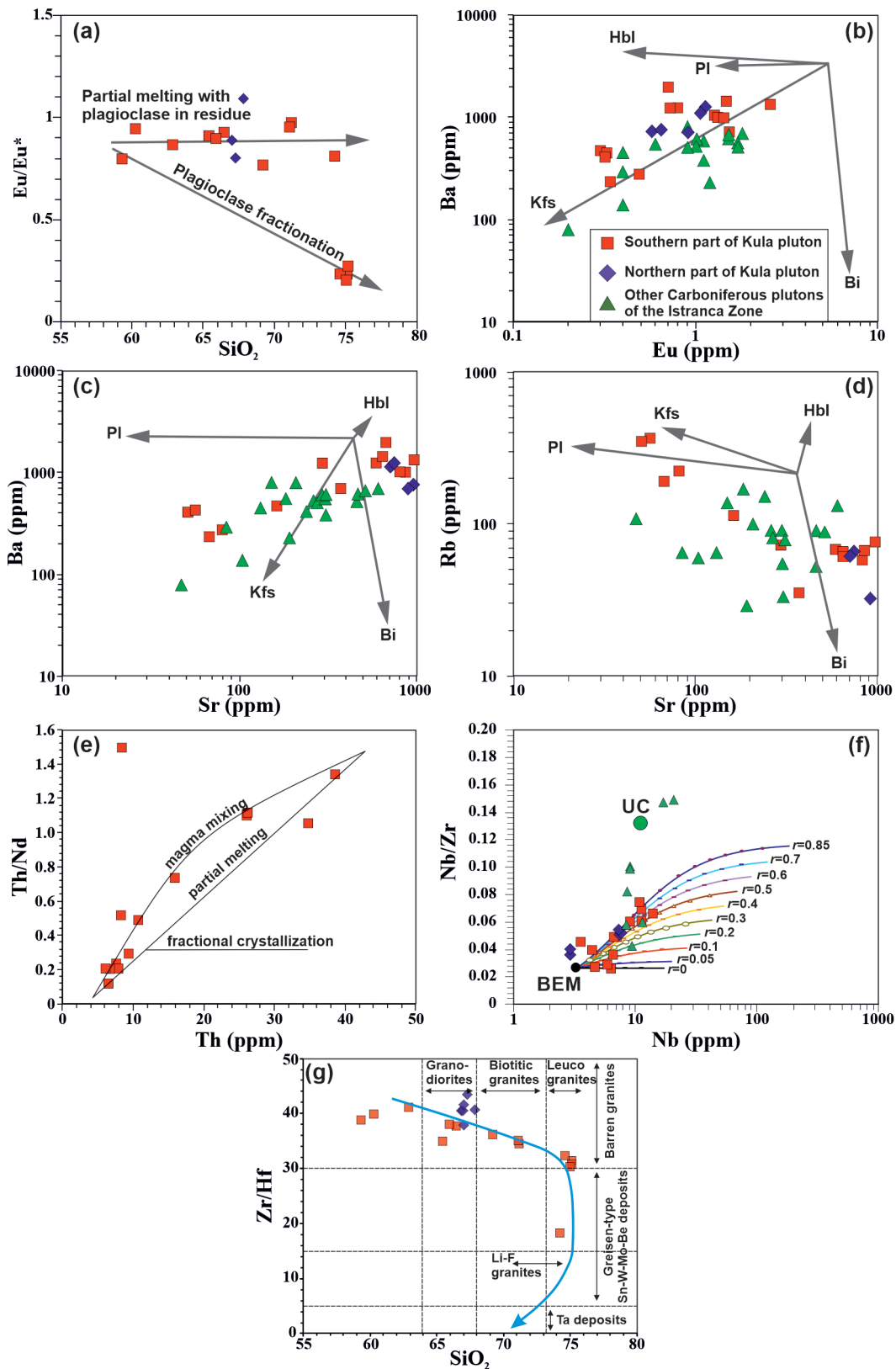
Fig. 9. Eu/Eu* vs. SiO2 (**a**), Ba vs. Eu (**b**), Ba vs. Sr (**c**), Rb vs. Sr (**d**), Th/Nd vs. Th (**e**) (after Schiano et al. 2010), Nb/Zr vs. Nb (**f**), and Zr/Hf vs. SiO2 (**g**) (after Zaraisky et al. 2008) binary plots for monitoring fractional crystallization, magma mixing, partial melting, and assimilation-fractional crystallization processes. Abbreviations: UC=Upper Crust, BEM=Basic end member, Hbl=hornblende, Pl=plagioclase, Kfs=K-feldspar, Bi=biotite.

mixtures, with trends suggesting the possible involvement of felsic components (Fig. 10a, b). On the $Al_2O_3/(FeO_T+MgO)$ $-3*CaO-5*(K_2O/Na_2O)$ ternary diagram (Laurent et al. (2014), the Kula pluton samples fall mainly into the field of partial melting of low-K mafic rocks and tonalite fields, and some of the samples fall into the field of partial melting of high-K mafic rocks and metasediments fields (Fig. 10c). Similarly, on the F–An–Or diagram (Castro 2013), all samples coherent with the low-pressure water-undersaturated granites field derived from the primary andesitic magma (Fig. 10d).

As a result, geochemical data for the studied plutonic rocks imply that these plutons formed by a crustal-derived mafic melts in a subduction-related tectonic settings at the lower–upper crust. These rocks mixed with sub continental lithospheric mantle and/or mafic lower crustal melts and were contaminated by felsic crustal melts.

Regional comparisons and geodynamics

The Permo–Carboniferous time was a geologically crucial time for Central Europe (including Rhodope, Serbo Macedonian, and Istranca Massifs), and Pontides (Schmid et al. 2020 and references therein). The Paleo-Tethys Ocean, which separated the Gondwana and Laurasia continents, underwent the last stages of subduction or closure in this period. Following the closure of the ocean, the Variscan orogeny developed in Europe with the collision of the Gondwana and Laurasia continents (Stampfli & Borel 2002; Cocks & Torsvik 2006; Okay & Topuz 2017). This orogen is characterized by the juxtaposition of blocks of continental crust where these Cadomian blocks are separated by high strain zones containing the record of subduction-related processes. These zones are interpreted as sutures between one or more postulated lithospheric microplates sandwiched between two major plates (Kroner & Romer 2013).

In Western and Central Europe, the Variscan orogeny ended in the Late Carboniferous with the collision of the main body of Gondwana with the amalgamated Laurussia (Tait et al. 1997; Stampfli & Borel 2002; Cocks & Torsvik 2006; Schulmann et al. 2014). The Variscan orogen in central Europe also involved Carboniferous low-pressure high-temperature (LP–HT) metamorphism and partial melting (Ivanov et al. 2000; von Quadt et al. 2006; Naydenov et al. 2009; Okay & Topuz 2017). These metamorphic rocks are closely associated
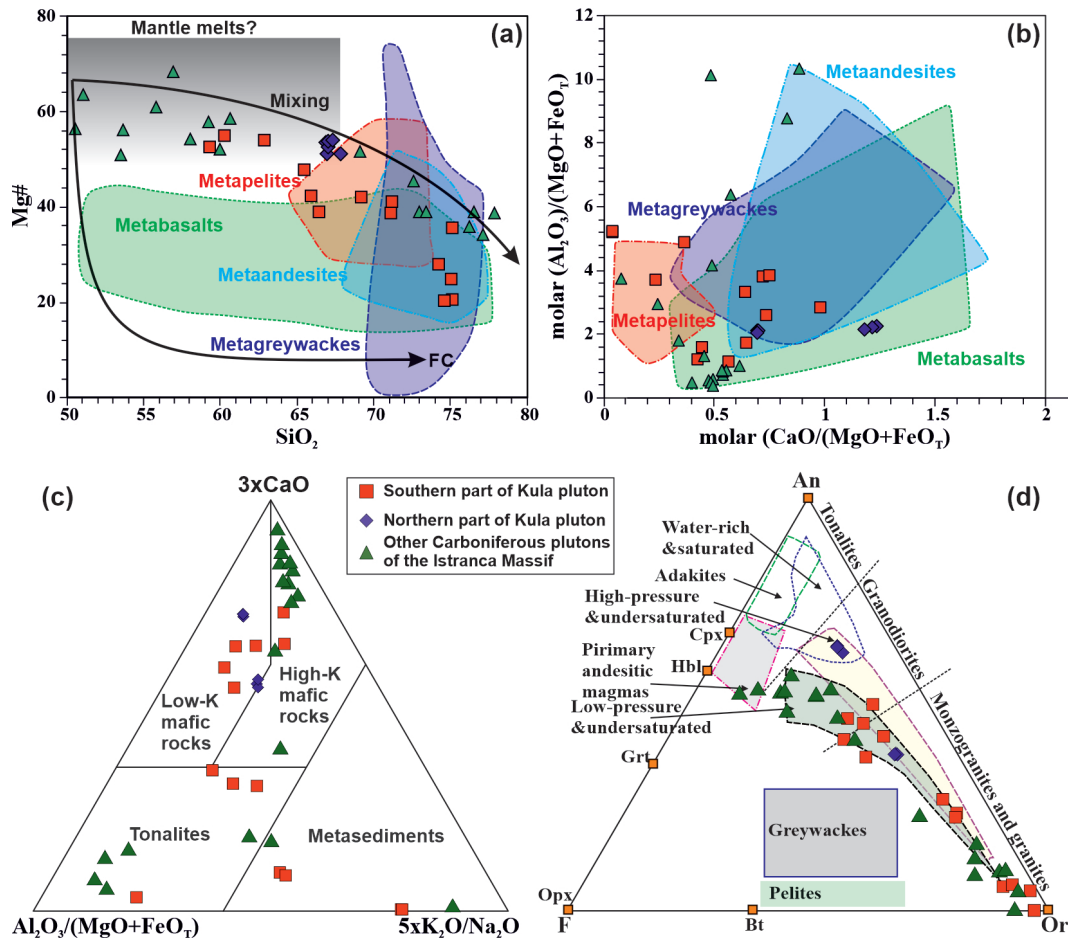

Fig. 10. Mg# vs. SiO_2 (**a**), and molar $Al_2O_3/(MgO+FeO_T)$ vs. $CaO/(MgO+FeO_T)$ (**b**) diagrams of Altherr & Siebel (2002); $Al_2O_3/(FeO_T+MgO)$ $-3*CaO-5*(K_2O/Na_2O)$ ternary diagram of Laurent et al. (2014) (**c**), and F–An–Or ternary diagram of Castro (2013) (**d**) for the description of source of magma.

with syn- and post-tectonic granites. The metamorphism is restricted to a narrow range (340–325 Ma, e.g., Henk et al. 2000; O'Brien 2000; Carrigan et al. 2006; Mayringer et al. 2011; Okay & Topuz 2017) in the Black Sea region.

Late Carboniferous–early Permian (328 to 271 Ma) granitoid magmatism in the Central Europe, the Rhodopes, Serbo-Macedonian Massifs and Istranca Zone, is defined as different orogenic and subduction processes by some researchers (Dimitrov 1946; Zagorchev et al. 1973; Okay et al. 2001; Kamenov et al. 2002; Peytcheva et al. 2004, 2018; Carrigan et al. 2005; Carrigan et al. 2006; Sunal et al. 2006; Machev et al. 2015; Okay & Topuz 2017; Bonev et al. 2019a; Table 1). This zone may be correlated with Central Europe due to magmatism and metamorphism.

There are different opinions about the tectonic setting of plutons in the late Carboniferous–early Permian period, which outcrop in the Istranca Massif. While some studies suggest that these rocks are products of the Variscan orogeny following the closure of the Paleo-Tethys ocean (Okay et al. 2001; Sunal et al. 2006; Machev et al. 2015), others emphasize that these metagranitoids were an active continental arc magmatic developing on the northern edge of the Paleo-Tethys, north of the N-dipping and still open basin (Natal'in et al. 2016; Bonev et al. 2019a). In addition, recent studies of upper Carboniferous granitoids in the Sakarya Zone and the Afyon zone, located in north-western Turkey, indicate that these granitoids are from a magmatic arc environment associated with the subduction of the Paleo-Tethys ocean (Ustaömer et al. 2012; Candan et al. 2016). For the Variscan-related arc granites in the Pelagonian and Sakarya zones on the active southern margin of Laurasia, a dual subduction of Paleo-Tethys can be envisaged between early Carboniferous and late Permian (Candan et al. 2016). On the other hand, the late-Variscan orogeny in the Istranca massif in the eastern part of Europe was defined during the early Permian period (Okay et al. 2001). Early Permian zircon ages are obtained from both the deep-level granites and the surrounding gneisses and migmatites (Okay et al. 2001). Younger ages were found for the Kırklareli metagranite (268.3±2.1 Ma), Tepecik cataclastic granite at the eastern end of the Istranca massif and Sancaktepe granite in İstanbul Zone (249.4±1.5 Ma SHRIMP U–Pb for the Tepecik pluton and 257.3±1.5 Ma and 253.7±1.75 Ma for the Sancaktepe pluton; Aysal et al. 2018a). The ages obtained were compared to relatively younger ages (Yılmaz Şahin et al. 2009; Aysal et al. 2018a) at the most south-eastern part of the Istranca Zone of 249.4±1.5 Ma and 253.6±1.75 Ma. These middle Permian–Lower Triassic (268.3±2.1 Ma to 249.4 ±1.5 Ma) plutons were formed in a subduction-relating setting (Aysal et al. 2018a). In addition, younger ages (243–238 Ma; Bonev et al. 2019b) of Triassic magmatism were obtained from igneous rocks in the westernmost parts of the Sakar-Istranca zone in Bulgaria. This middle Triassic igneous activity, following the late Carboniferous–Permian magmatism, is linked to the northward subduction of the Paleo-Tethys Ocean (Bonev et al. 2019b). It can be interpreted that the continental arc magmatism was more effective in the Sakar-Istranca Zone

during the late Carboniferous–Middle Triassic and demonstrates that the Paleo-Tethys subduction under the Eurasia is still on-going at that time.

In previous studies, ages of 293.5±1.7 and 301.9±1.1 Ma were obtained from the continuation of the Kula pluton in Bulgaria (Machev et al. 2015), while an age of 271±11 Ma was reported for the metagranite in Turkey (Okay et al. 2001). In this study, concordia ages of 298.06±0.68 Ma (early Permian – Asselian) and 311.91±1.34 Ma (late Carboniferous – Pennsylvanian) were obtained with U–Pb methods for magmatic zircons (KL-6 and KL-2) from the Kula pluton in NW Turkey (Fig. 2). Since the KL-6 sample was subjected to moderate deformation, it has textural differences compared to the KL-2 sample. Furthermore, younger ages (298.06±0.68 Ma) than the KL-2 sample (311.91±1.34 Ma) were obtained, located in the older area in the centre (Fig. 11). Based on these geochronology data, the Kula pluton was affected by the Variscan orogeny and related tectonic events. As is known, the Variscan orogeny in Western and Central Europe consists of two phases; an early phase between 340 and 325 Ma, and a late phase between 315 and 290 Ma (Finger et al. 1997; Bonev et al. 2019a). Late Carboniferous–Permian igneous activity in the Istranca Massif was interpreted in terms of Variscan evolution involving metamorphism and plutonism comparable to Central Europe (Okay et al. 2001; Okay & Topuz 2017). These different ages (from 271 to 310 Ma; Fig. 10) for the granitoids of that pluton might be due to incremental growth and by subsequents plutonic phases. The pluton was formed by several different magma pulses following the metamorphism of the host rocks. 296–279 Ma Rb–Sr ages obtained from Carboniferous metagranitoids in the Istranca Zone indicate the metamorphism at the Carboniferous–Permian boundary (Sunal et al. 2011). Also, these igneous rocks were affected by the early Alpine metamorphism that progressed from amphibolite facies to greenschist facies during the Late Jurassic–Early Cretaceous period (Sunal et al. 2011; Bonev et al. 2020). The different magma pulses in Istranca zone, including granitoids in Bulgaria, can be partly defined according to dating results and some geological and geochemical properties. Contacts, enclaves or xenoliths of granitoids, which are the most important evidences of different magma pulses in the field, could not be observed due to effects of dense forest, matemorphism and alteration. However, geochemically, it was observed that some samples contained high Ba and Sr against low Rb (KL-1, 2, 6. 7, 8, 9, 10, 13, 14), while some samples, on the contrary, contained low Ba and Sr against high Rb (KL-3, 4, 5,11, 12). Further work is also needed to distinguish the textural differences among the magmatic pulses, i.e. fabric orientations and fabric types of the Kula pluton.

New geochemical and geochronological data indicate that the Kula pluton can be considered a product of a subduction-related tectonic setting to the north of Paleo-Tethys, which is commonly observed in the Istranca–Rhodope–Serbo-Macedonian Massifs, during the late Carboniferous–early Permian period (Fig. 12). According to these features, the Istranca

Massif may be also assigned to the late Paleozoic–early Mesozoic Silk Road Arc (Natal'in & Şengör 2005) evolving on the southern margin of Eurasia due to the northward subduction of the Paleo-Tethys. Arguments for such assumption provide the Ordovician granitoids in the Sakar–Strandja zone that has been reported (Bonev et al. 2019a). The products of this Ordovician magmatism developing in the back-arc environment also point to the existence of a subduction system during the Ordovician (Bonev et al. 2013). According to Bonev et al. (2021), Sakar–Istranca zone shows a continental arc major magmatic pulse in the late Carboniferous–Permian connected with Paleo-Tethys subduction. According to all these data, The Istranca Massif might be also interpreted as a fragment of the long-lived Ordovician–Triassic magmatic arc, which evolved on the northern side of the Paleo-Tethys.
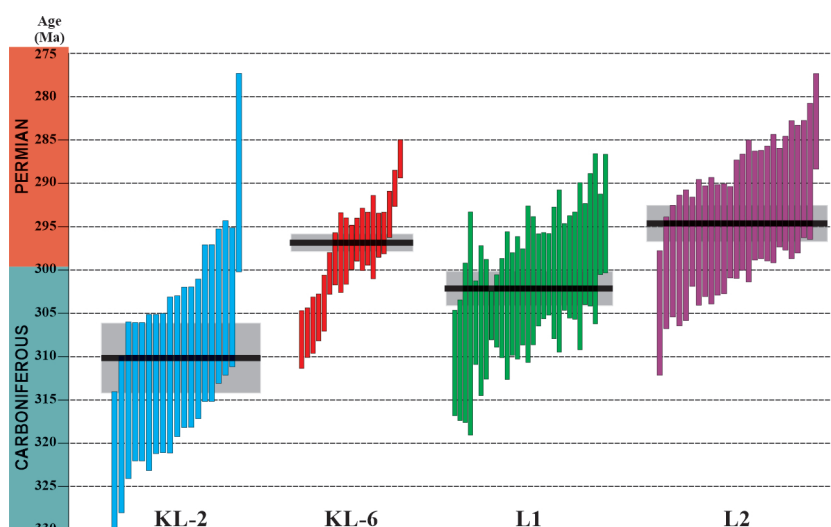

Fig. 11. Different age data from Kula pluton in Turkey (KL-2 and KL-6) and Bulgaria (L1 and L2; Machev et al. 2015).

Conclusion

Kula pluton has metaluminous, I-type, high-K calc-alkaline geochemical properties and it exhibits a hybrid magma character formed by fractional crystallization (FC) and magma mixing processes involving crustal and mantle material.

New U–Pb zircon ages of 298.06± 0.68 Ma (early Permian – Asselian) and 311.91±1.34 Ma (late Carboniferous – Pennsylvanian) were obtained from Kula pluton in the north-western part of the Istranca massif along the Turkey–Bulgaria border.

The different ages of the pluton might be due to incremental growth and subsequent plutonic phases that differ in age but postdate the metamorphism of the host rocks.

Kula pluton in the Istranca Zone shows similar composition, tectonic and geodynamic setting to other granitoids of NW Anatolia (Sakarya and Afyon Zones) and SE of Central europe (Serbo-Macedonian and Rhodope zones). All these granitoids formed along the active continental margin of the Eurasian plate related to subduction of Paleo-Tethys oceanic lithosphere.
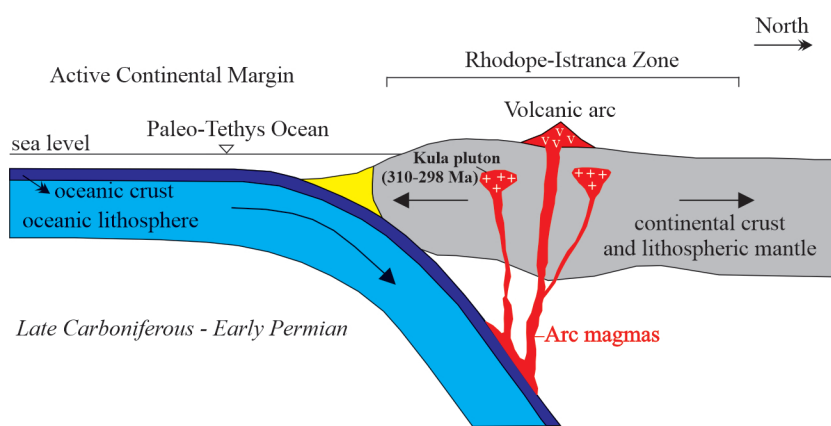
Fig. 12. Geodynamic model for late Carboniferous–early Permian evolution of the northern margin of the Paleo-Tethys.

References

Abalos B., Carreras J., Escuder-Viruete J. & Gomez-Pugnaire T. 2002: Variscan and Pre-Variscan Tectonics. In: The Geology of Spain. *The Geological Society of London*, 155–183.

Akgündüz S. 2017: Istranca Masifi'nin Batı Kesimlerinde (Kırklareli Kuzeyi) Mesozoyik-Erken Senozoyik Tektonizmasi ve Jeolojik Evrimi. *PhD thesis*, *Istanbul University Institute of Science*, 1–235 (in Turkish).

Altherr R. & Siebel W. 2002: I-type plutonism in a continental back-arc setting: Miocene granitoids and monzonites from the central Aegean Sea, Greece. *Contributions to Mineralogy and Petrology* 143, 397–415. https://doi.org/10.1007/s00410-002-0352-y

Altherr R., Holl A., Hegner E., Langer C. & Kreuzer H. 2000: High-potassium, calc-alkaline I-type plutonism in the European Variscides: northern Vosges (France) and northern Schwarzwald (Germany). *Lithos* 50, 51–73. https://doi.org/10.1016/S0024-4937(99)00052-3

Anders B., Reischmann T. & Kostopoulos D. 2007: Zircon geochronology of basement rocks from the Pelagonian Zone, Greece: constraints on the pre-Alpine evolution of the westernmost internal Hellenides. *International Journal of Earth Sciences* 96, 639–661. https://doi.org/10.1007/s00531-006-0121-7

Anderson A.T. 1976: Magma mixing petrological process and volcanological tool. *Journal of Volcanology and Geothermal Research* 1, 3–33.

Aydın Y. 1974: Petrographic and geochemical study of the central part of the Istranca Massif (Turkey). *PhD thesis*, *Nancy-Université*, 1–131 (in French).

Aydın Y. 1982: Geology of the Yıldız (Istranca) Mountains. *Associate Professor thesis*, *Istanbul Technical University*, 1–106.

Aysal N., Ustaömer T., Öngen S., Keskin M., Köksal S., Peytcheva I. & Fanning M. 2012a: Origin of the Early–Middle Devonian magmatism in the Sakarya Zone, NW Turkey: Geochronology, geochemistry and isotope systematics. *Journal of Asian Earth Sciences* 45, 201–222. https://doi.org/10.1016/j.jseaes.2011.10.011

Aysal N., Öngen S., Peytcheva I. & Keskin M. 2012b: Origin and evolution of the Havran Unit, Western Sakarya basement (NW Turkey): new LA-ICP-MS U–Pb dating of the metasedimentary–metagranitic rocks and possible affiliation to Avalonian microcontinent. *Geodinamica Acta* 25, 226–247. https://doi.org/10.1080/09853111.2014.882536

Aysal N., Yılmaz Şahin S., Güngör Y., Peytcheva I. & Öngen S. 2018a: Middle Permian–early Triassic magmatism in the Western Pontides, NW Turkey: Geodynamic significance for the evolution of the Paleo-Tethys. *Journal of Asian Earth Sciences* 164, 83–103. https://doi.org/10.1016/j.jseaes.2018.06.026

Aysal N., Keskin M., Peytcheva I. & Duru O. 2018b: Geochronology, geochemistry and isotope systematics of a Mafic-Intermediate Dyke Complex in the İstanbul Zone. New constraints on the evolution of Black Sea in NW Turkey. In: Simmons M.D., Tari G.C. & Okay A.I. (Eds.): Petroleum Geology of the Black Sea. *Geological Society of London, Special Publications* 464, 131–168.

Bedi Y., Vasilev E., Dabovski C., Ergen A., Okuyucu C., Doğan A., Kağan Tekin U., Ivanova D., Boncheva I., Lokova I., Sachanski V., Kuşcu I., Tuncay E., Demiray G.D., Soycan H. & Göncüoğlu M.C. 2013: New age data from the tectonostratigraphic units of the Istranca "Massif" in NW Turkey: a correlation with SE Bulgaria. *Geologica Carpathica* 64, 255–277. https://doi.org/10.2478/geoca-2013-0019

Bonev N., Ovtcharova-Schaltegger M., Moritz R., Marchev P. & Ulianov A. 2013: Peri-Gondwanan Ordovician crustal fragments in the high-grade basement of the Eastern Rhodope Massif, Bulgaria: evidence from U–Pb LA-ICP-MS zircon geochronology and geochemistry. *Geodinamica Acta* 26, 207–229. https://doi.org/10.1080/09853111.2013.858942

Bonev N., Filipov P., Raicheva R. & Moritz R. 2019a: Timing and tectonic significance of Paleozoic magmatism in the Sakar unit of the Sakar-Strandzha Zone, SE Bulgaria. *International Geology Review*. https://doi.org/10.1080/00206814.2019.1575090

Bonev N., Filipov P., Moritz R. & Raicheva R. 2019b: Triassic magmatism along the Maritsa river valley, Sakar-Strandzha zone. *Review of the Bulgarian Geological Society* 80, 56–57.

Bonev N., Spikings R. & Moritz R. 2020: ^{40}Ar/^{39}Ar age constraints for an early Alpine metamorphism of the Sakar unit, Sakar-Strandzha zone, Bulgaria. *Geological Magazine* 157, 2106–2112. https://doi.org/10.1017/S0016756820000953

Bonev N., Filipov P., Raicheva R. & Moritz R. 2021: Evidence of late Palaeozoic and Middle Triassic magmatism in the Sakar-Strandzha Zone, SE Bulgaria: Regional geodynamic implications. *International Geology Review*. https://doi.org/10.1080/00206814.2021.1917008

Burchfiel B.C. 1980: Eastern European Alpine system and the Carpathian orocline as an example of collision tectonics. *Tectonophysics* 63, 31–61.

Burg J.P., Ivanov Z., Ricou L.E., Dimor D. & Klain L. 1990: Implications of shear-sense criteria for the tectonic evolution of the Central Rhodope massif, southern Bulgaria. *Geology* 18, 451–454.

Burg J.P., Ricou L.E., Ivanov Z., Dimov D. & Klain L. 1996: Synmetamorphic nappe complex in the Rhodope Massif. Structure and kinematics. *Terra Nova* 8, 6–15.

Çağlayan M.A. & Yurtsever A. 1998: 1/100,000 scaled Turkey Geological Maps, Burgaz-A3, Edirne-B2 ve B3; Burgaz-A4 ve Kırklareli-B4; Kırklareli B5 ve B6; Kırklareli-C6 quadrangles. *General Directorate of Mineral Research and Exploration* (in Turkish).

Candan O., Akal C., Koralay O.E., Okay A.I., Oberhänsli R., Prelević D. & Mertz Kraus R. 2016: Carboniferous granites on the northern margin of Gondwana, Anatolide-Tauride Block, Turkey – Evidence for southward subduction of Paleo-Tethys. *Tectonophysics* 683, 349–366. https://doi.org/10.1016/j.tecto.2016.06.030

Carrigan C., Mukasa S., Haydoutov I. & Kolcheva K. 2005: Age of Variscan magmatism from the Balkan sector of the orogen, central Bulgaria. *Lithos* 82, 125–147. https://doi.org/10.1016/j.lithos.2004.12.010

Carrigan C., Mukasa S., Haydoutov I. & Kolcheva K. 2006: Neoproterozoic magmatism and Carboniferous high-grade metamorphism in Sredna Gora Zone, Bulgaria: an extension of the Gondwana derived Anatolia-Cadomian belt. *Gondwana Research* 147, 404–416.

Castro A. 2013: Tonalite–granodiorite suites as cotectic systems: a review of experimental studies with applications to granitoid petrogenesis. *Earth Science Reviews* 124, 68–95. https://doi.org/10.1016/j.earscirev.2013.05.006

Castro A., Gerya T., García-Casco A., Fernández C., Díaz Alvarado J., Moreno-Ventas I. & Loew I. 2010: Melting relations of MORB-sediment mélanges in underplated mantle wedge plumes. Implications for the origin of cordilleran-type batholiths. *Journal of Petrology* 51, 1267–1295. https://doi.org/10.1093/petrology/egq019

Chappell B.W. & White A.J.R. 1992: I- and S-type granites in the Lachlan Fold Belt. *Transactions of the Royal Society of Edinburgh, Earth Sciences* 83, 1–26.

Chatalov G.A. 1988: Recent developments in the geology of the Strandzha zone in Bulgaria. *Bulletin of the Technical University of Istanbul* 41, 433–465.

Chatalov A.G. 1991: Triassic in Bulgaria – a review. In: Dewey J.F. (Ed.): *Bulletin of the Technical University of Istanbul* 44, 103–135.

Chen F., Siebel W., Satır M., Terzioğlu N. & Saka K. 2002: Geochronology of the Karadere basement (NW Turkey) and implications for the geological evolution of the İstanbul zone. *International Journal of Earth Sciences* 91, 469–481. https://doi.org/10.1007/s00531-001-0239-6

Cocks L.R.M. & Torsvik T.H. 2006: European geography in a global context from the Vendian to the end of the Palaeozoic. In: Gee D.G. & Stephenson R.A. (Eds.): European lithosphere dynamics. *Geological Society, London, Memoirs* 32, 83–95.

Corfu F., Hanchar J., Hoskin P. & Kinny P. 2003: Atlas of Zircon Textures. *Reviews in Mineralogy and Geochemistry* 53, 469–500. https://doi.org/10.2113/0530469

Cortesogno L., Gaggero L., Ronchi A. & Yanev S. 2004: Late orogenic magmatism and sedimentation within Late Carboniferous to Early Permian basins in the Balkan terrane (Bulgaria): geodynamic implications. *International Journal of Earth Sciences* 93, 500–520. https://doi.org/10.1007/s00531-004-0410-y

Delaloye M. & Bingöl E. 2000. Granitoids from Western and Northwestern Anatolia: geochemistry and modeling of geodynamic

evolution. *International Geology Review* 42, 241–268. https://doi.org/10.1080/00206810009465081

Dias R. & Ribeiro A. 1995: The Ibero-Armorican Arc: A collisional effect against an irregular continent. *Tectonophysics* 246, 113–128.

Dimitrov S. 1946: The metamorphic and magmatic rocks of Bulgaria. *Ann. Comm. Geol. Inv.* 4, 61–93 (in Bulgarian).

Dinter D.A. & Royden L. 1993: Late Cenozoic extension in northeastern Greece: Strymon valley detachment system and Rhodope metamorphic core complex. *Geology* 21, 45–48.

Finger F., Roberts M., Haunschmid B., Schermaier A. & Steyrer H. 1997: Variscan granitoids of Central Europe: their typology, potential sources and tectonothermal relations. *Mineralogy and Petrology* 61, 67–96.

Henk A., von Blanckenburg F., Finger F., Schaltegger U. & Zulauf G. 2000: Syn-convergent high-temperature metamorphism and magmatism in the Variscides: a discussion of potential heat sources. In: Franke W., Haak V., Oncken O. & Tanner D. (Eds.): Orogenic processes: quantification and modelling in the Variscan belt. *Geological Society, London, Special Publications* 179, 387–399.

Hoskin P. & Schaltegger U. 2003: The Composition of Zircon and Igneous and Metamorphic Petrogenesis. *Reviews in Mineralogy and Geochemistry* 53, 27–62. https://doi.org/10.2113/0530027

Ivanov Z., Dimov D., Dobrev S., Kolkovski B. & Sarov S. 2000: Structure, alpine evolution and mineralizations of the Central Rhodopes area (South Bulgaria). In: Ivanov Z. (Ed.): Guide to Excursion B, ABCD-GEODE 2000 Workshop, Borovets, Bulgaria, vol. 50.

Kamenov B.K., von Quadt A. & Peytcheva I. 2002: New insight into petrology, geochemistry and dating of the Vejen pluton, Bulgaria. *Geochemistry, Mineralogy and Petrol*ogy 39, 3–25.

Karacık Z. & Tüysüz O. 2010: Petrogenesis of the Late Cretaceous Demirköy Igneous Complex in the NW Turkey: Implications for magma genesis in the Strandja Zone. *Lithos* 114, 369–384.

Karslı O., Şengün F., Dokuz A., Kandemir R., Aydın F. & Andersen T. 2020: Silurian to Early Devonian arc magmatism in the western Sakarya Zone (NWTurkey), with inference to the closure of the Rheic Ocean. *Lithos* 370–371, 1–18. https://doi.org/10.1016/j.lithos.2020.105641

Keskin M. 2002: FC-modeler: A Microsoft® Excel© spreadsheet program for modeling Rayleigh fractionation vectors in closed magmatic systems. *Computers & Geosciences* 28, 919–928. https://doi.org/10.1016/S0098-3004(02)00010-9

Keskin M. 2013: AFC-Modeler: A Microsoft® Excel© workbook program for modelling assimilation combined with fractional crystallization (AFC) process in magmatic systems by using equations of DePaolo (1981). *Turkish Journal of Earth Sciences* 22, 304–319. https://doi.org/10.3906/YER-1110-3

Kroner U. & Romer R.L. 2013: Two plates-Many subduction zones: The Variscan orogeny reconsidered. *Gondwana Res*earch 24, 298–329. https://doi.org/10.1016/j.gr.2013.03.001

Kuno H. 1950: Petrology of Hakone Volcano and adjacent areas, Japan. *Bulletin of the Geological Society of America* 61, 957–1020.

Laurent A., Janoušek V., Magna T., Schulmann K. & Míková J. 2014: Petrogenesis and geochronology of a post-orogenic calc-alkaline magmatic association: the Žulová Pluton, Bohemian Massif. *Journal of Geosciences* 59, 415–440. https://doi.org/10.3190/jgeosci.176

Liati A. 1986: Regional metamorphism and overprinting contact metamorphism of the Rhodope zone, near Xanthi, N. Greece: petrology, geochemistry, geochronology. *Dissertation thesis*, *Technical University Braunschweig*, 1–186.

Liati A. & Gebauer D. 1999: Constraining the prograde and retrograde P–T–t path of Eocene HP-rocks by SHRIMP dating of different zircon domains: inferred rates of heating, burial, cooling and exhumation for central Rhodope, northern Greece. *Contributions to Mineralogy and Petrology* 135, 340–354.

Machev P., Ganev V. & Klain L. 2015: New LA-ICP-MS U–Pb zircon dating for Istranca granites (SE Bulgaria): evidence for twostage late Variscan magmatism in the internal Balkanides. *Turkish Journal of Earth Sciences* 24, 230–248. https://doi.org/10.3906/yer-1407-21

Maniar P.D. & Piccoli P.M. 1989: Tectonic discrimination of granitoids. *Bulletin of the American Geological Soci*ety 101, 635-643.

Martinez Catalan J.R., Aller J. & Bastida F. 2009: The Iberian Variscan orogeny. In: *Contextos geológicos españoles*, 13–30.

Mayringer F., Treloar J., Gerdes A., Finger F. & Shengelia D. 2011: New age data from the Dzirula Massif, Georgia: implications for the evolution of the Caucasian Variscides. *American Journal of Science* 311, 404–441.

Middlemost E.A.K. 1994: Naming materials in magma/igneous rock system. *Earth Science Reviews* 37, 215–224.

Natal'in B.A. 2006: Paleozoic evolution of the northern margin of Paleo-Tethys. In: Tomurhuu D., Natal'in B., Ariunchimeg Y., Khishigsuren S. & Erdenesaikhan G. (Eds.): Second International Workshop and Field Excursions for IGCP Project-480. Structural and Tectonic correlation across the Central Asian Orogenic Collage: Implications for Continental Growth and Intracontinental Deformation. Abstracts and Excursion Guide Book: Ulaanbaatar. *Institute of Geology and Mineral Recourses, Mongolian Academy of Sciences*. 33-36.

Natal'in B.A. & Şengör A.M.C. 2005: Late Palaeozoic to Triassic evolution of the Turan and Scythian platforms: the pre-history of the Palaeo-Tethyan closure. *Tectonophysics* 404, 175–202. https://doi.org/10.1016/j.tecto.2005.04.011

Natal'in B.A., Sunal G. & Toraman E. 2005a: The Istranca arc: anatomy of collision after long-lived arc parallel tectonic transport. In: Sklyarov E.V. (Ed.): Structural and Tectonic Correlation across the Central Asia Orogenic Collage: North-Eastern Segment. *Guidebook and abstract volume of the Siberian Workshop IGCP-480: Irkutsk, IEC SB RAS*, 240–245.

Natal'in B.A., Satır M., Sunal G. & Toraman E. 2005b: Structural and metamorphic evolution of the Istranca massif. Final report of the 101Y010 Project. *Türkiye Bilimsel Teknik Araştırma Kurumu, Yer Deniz Atmosfer Bilimleri ve Çevre Araştırma Grubu*, 1–183 (in Turkish).

Natal'in B.A., Sunal G., Satır M. & Toraman E. 2012: Tectonics of the Istranca Massif, NW Turkey: History of a long-lived arc at the northern margin of Paleo-Tethys. *Turkish Journal of Earth Sciences* 21, 755–798.

Natal'in B.A., Sunal G., Gün E., Wang B. & Zhiqing Y. 2016: Precambrian to Early Cretaceous rocks of the Strandja Massif (northwestern Turkey): evolution of a long lasting magmatic arc. *Canadian Journal of Earth Sciences* 53, 1312–1335. https://doi.org/10.1139/cjes-2016-0026

Naydenov K., Von Quadt A., Peytcheva I., Sarov S. & Dimov D. 2009: U–Pb zircon dating of metamorphic rocks in the region of Kostenets-Kozarsko villages: constraints on the tectonic evolution of the Maritsa strike-slip shear zone. *The Review of the Bulgarian Geological Society* 70, 5–21.

O'Brien P.J. 2000: The fundamental Variscan problem: high temperature metamorphism at different depths and high-pressure metamorphism at different temperatures. In: Franke W., Haak V., Oncken O. & Tanner D. (Eds.): Orogenic processes: quantification and modelling in the Variscan Belt. *Geological Society, London, Special Publications* 179, 369–386.

Okay A.I. & Nikishin A.M. 2015: Tectonic evolution of the southern margin of Laurasia in the Black Sea region. *International Geology Review* 57, 1051–1076. https://doi.org/10.1080/00206814.2015.1010609

Okay A.I. & Topuz G. 2017: Variscan orogeny in the Black Sea region. *International Journal of Earth Sciences* 106, 569–592. https://doi.org/10.1007/s00531-016-1395-z

Okay A.I. & Tüysüz O. 1999: Tethyan sutures of northern Turkey. In: Durand B., Jolıvet L., Horvath F. & Seranne M. (Eds.): The Mediterranean Basins: Tertiary Extension within the Alpine Orogen. *Geological Society Special Publication* 156, 475–515.

Okay A.I., Satır M., Maluski H., Siyako M., Monie P., Metzger R. & Akyüz S. 1996: Paleo- and Neo-Tethyan events in northwestern Turkey: geologic and geochronologic constraints. In: Yin A. & Harrison M. (Eds.): The tectonic evolution of Asia. *University Press Cambridge*, Cambridge, 420–441.

Okay A.I., Satır M., Tüysüz O., Akyuz S. & Chen F. 2001: The tectonics of the Istranca Massif: late-Variscan and mid-Mesozoic deformation and metamorphism in the northern Aegean. *International Journal of Earth Sciences* 90, 217–233.

Okay A.I., Satır M. & Siebel W. 2006: Pre-Alpide Palaeozoic and Mesozoic orogenic events in the Eastern Mediterranean region. *Geological Society, London, Memoirs* 32, 389–405. https://doi.org/10.1144/GSL.MEM.2006.032.01.23

Okay A.I., Bozkurt E., Satır M., Yiğitbaş E., Crowley Q.G. & Shang C.K. 2008. Defining the southernmargin of Avalonia in Pontides: geochronological data from the Late Proterozoic and Ordovician granitoids from NW Turkey. *Tectonophysics* 461, 252–264.

Okay N., Zack T., Okay A.I. & Barth M. 2011: Sinistral transport along the Trans-European Suture Zone: detrital zircon–rutile geochronology and sandstone petrography from the Carboniferous flysch of the Pontides. *Geological Magazine* 148, 380–403. https://doi.org/10.1017/S0016756810000804

Patiño Douce A.E. 1999: What do experiments tell us about the relative contributions of crust and mantle to the origin of granitic magmas? *Geological Society Special Publication* 168, 55–75.

Pearce J.A., Harris N.B.W. & Tindle A.G. 1984: Trace element discrimination diagrams for the tectonic interpretation of granitic rocks. *Journal of Petrology* 25, 956–983.

Peccerillo R. & Taylor S.R. 1976: Geochemistry of Eocene calc-alkaline volcanic rocks from the Kastamonu area. Northern Turkey. *Contributions to Mineralogy and Petrology* 58, 63–81.

Peytcheva I., von Quadt A., Ovtcharova M., Handler R., Neubauer F., Salnikova E., Kostitsyn Y., Sarov S. & Kolcheva K. 2004: Metagranites from the eastern part of the Central Rhodopean Dome (Bulgaria): U–Pb, Rb–Sr and ^{40}Ar/^{39}Ar timing of emplacement and exhumation and isotope-geochemical features. *Mineralogy and Petrology* 82, 1–31. https://doi.org/10.1007/s00710-004-0039-3

Peytcheva I., von Quadt A., Tarassov M., Zidarov N., Tarassova E. & Andreichev V. 2009: Timing of Igralishte pluton in Ograzhden Mountain, SW Bulgaria: implications for the tectono-magmatic evolution of the region. *Geologica Balcanica* 38, 5–14.

Peytcheva I., Tacheva E., Quadt A. & Nedialkov R. 2018: U–Pb zircon and titanite ages and Sr-Nd-Hf isotope constraints on the timing and evolution of the Petrohan-Mezdreya pluton (Western Balkan Mts, Bulgaria). *Geologica Balcanica* 47, 25–46.

Pidgeon R.T. 1992: Recrystallization of oscillatory zoned zircon: some geochronological and petrological implications. *Contributions to Mineralogy and Petrology* 110, 463–472.

Pidgeon R.T., Nemchin A.A. & Hitchen G.J. 1998: Internal structures of zircon from Archean granites from the Darling Range batholith: implications for zircon stability and the interpretation of zircon U–Pb ages. *Contributions to Mineralogy and Petrology* 132, 288–299.

Ricou L.E., Burg J.P., Godfriaux I. & Ivanov Z. 1998: Rhodope and Vardar: the metamorphic and the olistostromic paired belts related to the Cretaceous subduction under Europe. *Geodinamica Acta* 11, 285–309.

Rudnick R.L. & Gao S. 2003: Composition of the Continental Crust. *Treatise on Geochemistry* 3, 1–64. https://doi.org/10.1016/B0-08-043751-6/03016-4

Schandl E.S. & Gorton M.P. 2002: Application of high field strength elements to discriminate tectonic settings in VMS environments. *Economic Geology* 97, 629–642. https://doi.org/10.2113/gsecongeo.97.3.629

Schiano P., Monzier M., Eissen J.P., Martin H. & Koga K.T. 2010: Simple mixing as the major control of the evolution of volcanic suites in the Ecuadorian Andes. *Contributions to Mineralogy and Petrology* 160, 297–312. https://doi.org/10.1007/s00410-009-0478-2

Schmid S.M., Fügenschuh B., Kounov A., Matenco L., Nievergelt P., Oberhansli R., Pleuger J., Schefer S., Schuster R., Tomljenovic B., Ustaszewski K. & van Hinsbergen D.J.J. 2020: Tectonic units of the Alpine collision zone between Eastern Alps and western Turkey. *Gondwana Research* 78, 308–374. https://doi.org/10.1016/j.gr.2019.07.005

Schulmann K., Martinez Catalan J.R., Lardeaux J.M., Janoušek V. & Oggiano G. 2014: The Variscan orogeny: Extent, timescale and the formation of the European crust. *Geological Society, London, Special Publications* 405, 1–6. https://doi.org/10.1144/SP405.15

Şengün F., Koralay O.E. & Kristoffersen M. 2020: Zircon U–Pb age and Hf isotopic composition of the Carboniferous Gönen granitoid in the western Sakarya Zone of Turkey. *Turkish Journal of Earth Sciences* 29, 617–628. https://doi.org/10.3906/yer-1910-7

Shand S.J. 1947: Eruptive Rocks, Their Genesis, Composition, Classification, and Their Relation to Ore-deposits, Third edition. *John Wiley and Sons*, New York, 1–488.

Stampfli G.M. & Borel G.D. 2002: A plate tectonic model for the Paleozoic and Mesozoic constrained by dynamic plate boundaries and restored synthetic oceanic isochrons. *Earth and Planetary Science Letters* 196, 17–33. https://doi.org/10.1016/S0012-821X(01)00588-X

Streckeisen A. 1974: Classification and nomenclature of plutonic rocks. *Geologische Rundschau* 63, 773–786.

Sun W. & McDonough W.F. 1989: Chemical and isotopic systematics of oceanic basalts: Implications for mantle composition and processes. *Geological Society, London, Special Publications* 42, 313–345.

Sunal G. 2012: Devonian magmatism in the western Sakarya Zone, Karacabey region, NW Turkey. *Geodinamica Acta* 25, 183–201. https://doi.org/10.1080/09853111.2013.858947

Sunal G., Natal'in B.A., Satır M. & Toraman E. 2006: Palaeozoic magmatic events in the Istranca Massif, NW Turkey. *Geodinamica Acta* 19, 281–298. https://doi.org/10.3166/ga.19.283-300

Sunal G., Satır M., Natal'in B.A., Topuz G. & Vonderschmidt O. 2011: Metamorphism and diachronous cooling in a contractional orogen: The Istranca Massif, NW Turkey. *Geological Magazine* 148, 580–594. https://doi.org/10.1017/S0016756810001020

Tait J.A., Bachtadse V., Franke W. & Soffel H.C. 1997: Geodynamic evolution of the European Variscan fold belt: palaeomagnetic and geological constraints. *Geologische Rundschau* 86, 585–598.

Topuz G., Candan O., Okay A.I., von Quadt A., Othman M., Zack T. & Wang J. 2020: Silurian anorogenic basic and acidic magmatism in Northwest Turkey: Implications for the opening of the Paleo-Tethys. *Lithos* 356–357, 1–14. https://doi.org/10.1016/j.lithos.2019.105302

Ustaömer P.A., Mundil R. & Renne P.R. 2005: U/Pb and Pb/Pb zircon ages for arc-related intrusions of the BoluMassif (W Pontides, NW Turkey): evidence for Late Precambrian (Cadomian) age. *Terra Nova* 17, 215–223. https://doi.org/10.1111/j.1365-3121.2005.00594.x

Ustaömer P.A., Ustaömer T. & Robertson A.H.F. 2012: Ion Probe U–Pb Dating of the Central Sakarya Basement: A peri-Gondwana

Terrane Intruded by Late Lower Carboniferous Subduction/Collision-related Granitic Rocks. *Turkish Journal of Earth Sciences* 21, 905–932.

Ustaömer T., Ustaömer P.A., Robertson A. & Roberson A.G. 2016: Implications of U–Pb and Lu–Hf isotopic analysis of detrital zircons for the depositional age, provenance and tectonic setting of the Permian-Triassic Palaeotethyan Karakaya Complex, NW Turkey. *International Journal of Earth Sciences* 105, 7–38. https://doi.org/10.1007/s00531-015-1225-8

von Quadt A., Sarov S., Peytcheva I., Voinova E., Petrov N., Nedkova K. & Naydenov K. 2006: Metamorphic rocks from northern parts of central Rhodopes – Conventional and in situ U–Pb zircon dating, isotope tracing and correlations. In: Proceedings National Conference Geosciences. *Bulgarian Geological Society*, Sofia, 225–228.

Vozárová A., Ebner F., Kovács S., Kräutner H-G., Szederkenyi T., Krstić B., Sremac J., Aljinovič D., Novak M. & Skaberne D. 2009: Late Variscan (Carboniferous to Permian) environments in the Circum Pannonian Region. *Geologica Carpathica* 60, 71–104. https://doi.org/10.2478/v10096-009-0002-7

Weil A.B., Van der Voo B. & Van der Pluijm B. 2001: Oroclinal bending and evidence against the Pangea megashear: The Cantabria-Asturias arc (northern Spain). *Geology* 29, 991–994. https://doi.org/10.1130/0091-7613(2001)029%3C0991:OBAEAT%3E2.0.CO;2

Yanev S. 2000: Paleozoic terranes of the Balkan Peninsula in the framework of Pangea asembly. *Palaeogeography, Palaeoclimatology, Palaeoecology* 161, 151–177. https://doi.org/10.1016/S0031-0182(00)00121-8

Yanev S. & Adamia S. 2009: General correlation of the Late Palaeozoic sequences in the Balkans and the Caucasus. *Journal of the Earth Sciences Application and Research Centre of Hacettepe University* 31, 1–22.

Yılmaz I., Yılmaz Şahin S., Aysal N., Güngör Y., Akgündüz A. & Bayhan U. 2021: Geochronology, geochemistry and tectonic setting of the Cadomian (Ediacaran–Cambrian) magmatism in the Istranca (Strandja) Massif: new insights into magmatism along the northern margin of Gondwana in NW Turkey. *International Geology Review*. https://doi.org/10.1080/00206814.2021.1901 249

Yılmaz Şahin S., Güngör Y., Aysal N. & Öngen S. 2009: Geochemistry and SHRIMP zircon U–Pb dating of granites within the Istranca and Istanbul Zones (NW Turkey). In: *62nd Geological Congress Turkey*, 598–599 (in Turkish).

Yılmaz Şahin S., Aysal N. & Güngör Y. 2012: Petrogenesis of Late Cretaceous adakitic magmatism in the İstanbul zone (Çavuşbaşı Granodiorite, NW Turkey). *Turkish Journal of Earth Sciences* 21, 1029–1045.

Yılmaz Şahin S., Aysal N., Güngör Y., Peytcheva I. & Neubauer F. 2014: Geochemistry and U–Pb zircon geochronology of metagranites in Istranca (Istranca) Zone, NW Pontides, Turkey: implications for the geodynamic evolution of Cadomian orogeny. *Gondwana Res*earch 26, 755–771.

Xypolias P., Dörr W. & Zulauf G. 2006: Late Carboniferous plutonism within the pre-Alpine basement of the External Hellenides (Kithira, Greece): Evidence from U-Pb zircon dating. *Journal of the Geological Society of London* 163, 539–547. https://doi.org/10.1144/0016-764904-114

Zagorchev I., Dabovski H. & Chunev D. 1973: On the tectonics of the western part of the Sredna Gora crystalline block (Sredna Gora proper). *Spisanie na Bulgarskogo Geologichesko Druzhestvo* 34, 1–10.

Zaraisky G.P., Aksyuk A.M., Devyatova V.N., Udoratina O.V., & Chevychelov V.Yu. 2008: Zr/Hf Ratio as an Indicator of Fractionation of Rare-Metal Granites by the Example of the Kukulbei Complex, Eastern Transbaikalia. *Petrology* 16, 710–736. https://doi.org/10.1134/S0869591108070047

Zlatkin O., Avigad D. & Gerdes A. 2014: Peri-Amazonian provenance of the Proto-Pelagonian basement (Greece), from zircon U–Pb geochronology and Lu–Hf isotopic geochemistry. *Lithos* 184, 379–392. https://doi.org/10.1016/j.lithos.2013.11.010

Zulauf G., Dörr W., Fisher-Spurlock S.C., Gerdes A., Chatzaras V. & Xypolias P. 2014: Closure of the Paleotethys in the External Hellenides: constraints from U-Pb ages of magmatic and detrital zircons (Crete). *Gondwana Research* 28, 642–667. https://doi.org/10.1016/j.gr.2014.06.011